

Characterization of thraustochytrid-specific sterol 0-acyltransferase: modification of DGAT2-like enzyme to increase the sterol production in *Aurantiochytrium limacinum* mh0186

Ishibashi, Yohei

Department of Bioscience and Biotechnology, Graduate School of Bioresource and Bioenvironmental Sciences, Kyushu University

Sadamitsu, Shohei

Department of Bioscience and Biotechnology, Graduate School of Bioresource and Bioenvironmental Sciences, Kyushu University

Fukahori, Yoshitomo

Department of Bioscience and Biotechnology, Graduate School of Bioresource and Bioenvironmental Sciences, Kyushu University

Yamamoto, Yuki

Department of Bioscience and Biotechnology, Graduate School of Bioresource and Bioenvironmental Sciences, Kyushu University

他

<https://hdl.handle.net/2324/7179471>

出版情報 : Applied and Environmental Microbiology. 89 (11), 2023-11-29. American Society for Microbiology

バージョン :

権利関係 : © 2023 Ishibashi et al.



Characterization of thraustochytrid-specific sterol O-acyltransferase: modification of DGAT2-like enzyme to increase the sterol production in *Aurantiochytrium limacinum* mh0186

Yohei Ishibashi,¹ Shohei Sadamitsu,¹ Yoshitomo Fukahori,¹ Yuki Yamamoto,¹ Rin Tanogashira,² Takashi Watanabe,¹ Masahiro Hayashi,³ Makoto Ito,¹ Nozomu Okino¹

AUTHOR AFFILIATIONS See affiliation list on p. 18.

ABSTRACT Thraustochytrids are marine microorganisms expected to produce useful lipids. They synthesize polyunsaturated fatty acids and sterols and store them in lipid droplets as a form of triacylglycerol (TG) and sterol ester (SE), respectively. TG is synthesized by diacylglycerol O-acyltransferase (DGAT). There are several DGAT2 homologs in *Aurantiochytrium limacinum*. This study indicated that DGAT2C and DGAT2D are SE synthase and TG synthase, respectively, by disrupting their corresponding genes in *A. limacinum* mh0186. DGAT2C is revealed as thraustochytrid-specific acyl-CoA:sterol-O-acyltransferase by performing *in vivo* and *in vitro* assays after heterologous expression in *Saccharomyces cerevisiae*. DGAT2C and DGAT2D localized mainly to the endoplasmic reticulum (ER) and the lipid droplet, respectively, and the two of the N-terminal domains unique to DGAT2C were essential for ER localization and SE synthesis in *A. limacinum* mh0186. Interestingly, the study also found that deletion of the first eight transmembrane domains in the unique N-terminal region of DGAT2C increased SE and total sterol productivity when expressed in DGAT2C-deficient *A. limacinum* mh0186. In addition, intermediates such as Δ^7 -cholesterol (provitamin D3) also accumulated in SE by expression of the N-terminal-truncated DGAT2C, along with cholesterol and Δ^7 -stigmasterol, a major phytosterol in *A. limacinum*. This study proves that DGAT2C is an ER-localized SE synthase and that its suitable N-terminal deletion can increase sterol production in thraustochytrids.

IMPORTANCE Since the global market for sterols and vitamin D are grown with a high compound annual growth rate, a sustainable source of these compounds is required to keep up with the increasing demand. Thraustochytrid is a marine oleaginous microorganism that can synthesize several sterols, which are stored as SE in lipid droplets. DGAT2C is an unconventional SE synthase specific to thraustochytrids. Although the primary structure of DGAT2C shows high similarities with that of DGAT, DGAT2C utilizes sterol as an acceptor substrate instead of diacylglycerol. In this study, we examined more detailed enzymatic properties, intracellular localization, and structure-activity relationship of DGAT2C. Furthermore, we successfully developed a method to increase sterol and provitamin D3 productivity of thraustochytrid by more than threefold in the process of elucidating the function of the DGAT2C-specific N-terminal region. Our findings could lead to sustainable sterol and vitamin D production using thraustochytrid.

KEYWORDS sterols, sterol ester, diacylglycerol, thraustochytrid, sterol o-acyltransferase, DGAT

Sterols are essential components of the cell membrane of eukaryotes and play an important role in regulating the physicochemical properties, such as membranous

Editor Isaac Cann, University of Illinois Urbana-Champaign, Urbana, Illinois, USA

Address correspondence to Yohei Ishibashi, ishibashiyo@agr.kyushu-u.ac.jp.

The authors declare no conflict of interest.

See the funding table on p. 18.

Received 15 June 2023

Accepted 4 September 2023

Published 24 October 2023

Copyright © 2023 Ishibashi et al. This is an open-access article distributed under the terms of the [Creative Commons Attribution 4.0 International license](https://creativecommons.org/licenses/by/4.0/).

strength, fluidity, and permeability, of cell membranes (1). In addition to these fundamental functions, plant sterols (phytosterols) are known to have biological benefits such as anti-inflammatory, anti-oxidant, and anti-cancer activities (2). High blood cholesterol level is a significant risk factor for cardiovascular disease, one of the major causes of death worldwide (3). Importantly, phytosterol can lower blood cholesterol by inhibiting the intestinal absorption of cholesterol (4, 5). Reducing blood cholesterol level by phytosterol is an effective way to reduce the risk of cardiovascular disease. Moreover, highly purified sterol is used as the component of lipid nanoparticles to deliver various therapeutics, such as mRNA, for vaccines against viral infections and cancer (6). Thus, the global market for phytosterols is expected to grow at a compound annual growth rate of 9.6% (5). Oils derived from corn, canola, and wood pulp are the primary sources of phytosterols. However, it has been a concern that terrestrial plants alone may be unable to keep up with the increasing demand for phytosterols because of limited agricultural land and the requirement for a large amount of fresh water. Therefore, alternative sources for sustainable sterol production are required.

Thraustochytrids are eukaryotic marine protists, including the typical genera *Aurantiochytrium*, *Aplanochytrium*, *Schizochytrium*, *Thraustochytrium*, and *Parietichytrium*, which belong to the Stramenopiles, class Labyrinthulomycetes, family Thraustochytriaceae (7–9). Thraustochytrids have recently received increasing attention from academic and industry experts because they produce considerable amounts of n-3 polyunsaturated fatty acids (n-3PUFA) such as docosahexaenoic acid (DHA, C22:6 n-3) (10). They accumulate n-3PUFAs and palmitic acid mainly as acyl chains of triacylglycerol (TG) in lipid droplets (LDs) and phosphatidylcholine (PC). In addition to n-3PUFA, several studies have shown that thraustochytrids can synthesize phytosterol (Δ^7 -stigmasterol) and cholesterol, which are stored as sterol ester (SE) in LDs (11, 12). Because the lipid productivity of thraustochytrids is higher (>50% dry cell weight) than that of terrestrial plants, this marine oleaginous microorganism is expected to be a sustainable source of nutritional lipids, n-3PUFAs, and sterols (13). A key advantage of using thraustochytrid to produce lipids is that they do not require agricultural land, unlike terrestrial plants, and are culturable in seawater, thus minimizing the use of potable fresh water with which scarcity is concerned because of climate change and population growth (5, 14). Since the productivity of sterols by thraustochytrid is insufficient for industrial use, effective methods to improve sterol production are required.

Acyl-CoA:diacylglycerol O-acyltransferase (DGAT), which transfers fatty acid from acyl-CoA to diacylglycerol (DG), is a key enzyme for TG synthesis in eukaryotes (15). DGAT is divided into the DGAT1, 2, and 3 families based on their sequence similarities. Lan et al. found that four DGAT2 homologs are present in *Aurantiochytrium*, tentatively named DGAT2A, B, C, and D (16). They showed that DGAT2A, C, and D are TG synthases by heterologous expression in budding yeast. A previous study also indicated that the mRNA expression level of *dgat2d* is higher than that of *dgat2a* and *dgat2c*, suggesting that *dgat2d* would be a major TG synthase in *A. limacinum* (16).

In this study, we examined the endogenous function of DGAT2 homologs in *A. limacinum* mh0186 and revealed that DGAT2C synthesizes SE by using acyl-CoA and sterols as substrates, and suitable deletion of N-terminal transmembrane regions of DGAT2C increased the sterol production, including phytosterols in *Aurantiochytrium limacinum* mh0186. Furthermore, expression of the N-terminal-deletion mutant in *A. limacinum* mh0186 produced Δ^7 -cholesterol-ester, which is rarely detected in wild-type (WT) *A. limacinum*.

MATERIALS AND METHODS

Strains and culture

A. limacinum mh0186 (17), isolated from seawater of the Yaeyama Islands in Okinawa, Japan, was grown in GY medium (3% glucose and 1% yeast extract in 1.75% artificial seawater) at 25°C with rotation at 150 rpm for the period indicated. Potato dextrose

agar (PDA) plates (50% potato dextrose, 1.75% artificial sea water, 2% agar) containing appropriate antibiotics were used to select the *dgat2a* knockout (KO), *dgat2c* KO, *dgat2d* KO, *dgat2c* KO/overexpression (OE), *dgat2c* OE, and N-terminal transmembrane regions deleted (Δ TM) *dgat2c*-expressing strains. The growth (biomass) of *A. limacinum* WT and transfected strains were monitored by measuring optical density at 600 nm (OD 600). The glucose concentration of the medium was measured by the Glucose CII test (FUJIFILM Wako Pure Chemical Co., Japan).

Materials

1,2-Diundecanoyl-*sn*-glycero-3-phosphocholine [PC22:0 (C11:0/C11:0)], 1,2-didocosa-hexaenoyl-*sn*-glycero-3-phosphocholine [PC44:12 (C22:6/C22:6)], docosahexaenoyl coenzyme A (C22:6-CoA), and 16:0 cholesteryl-d7 ester (d7-C16:0-CE) were purchased from Avanti Polar Lipids (AL, USA). TG36:0 (12:0/12:0/12:0) (Trilaurin) was purchased from Tokyo Chemical Industry (Tokyo, Japan). Antibodies against anti-DYKDDDDK tag (#2368) and anti-rabbit IgG horseradish peroxidase (HRP) were obtained from Cell Signaling Technology (MA, USA). SEALIFE, used as artificial seawater, was purchased from Nihonkaisui Co. (Tokyo, Japan). Thin-layer chromatography (TLC) plate was purchased from Merck Millipore (MA, USA).

Generation of *dgat2a*-, *dgat2c*-, or *dgat2d*-disrupted mutants

The genetic information of *dgat2a*, *dgat2c*, and *dgat2d* was obtained using the draft genome database provided by Joint Genome Institute. Genes encoding *dgat2a* (GenBank accession number: [MT762143](#)), *dgat2c* (GenBank accession number: [MF926506.1](#)), and *dgat2d* (GenBank accession number: [MF926507.1](#)) were disrupted by homologous recombination using a targeting construct (Fig. S1A through C) by the method described in reference (18). 5' and 3' homology arms of *dgat2a*, *dgat2c*, or *dgat2d* were amplified using the genomic DNA of *A. limacinum* as a template with primers described in Table S1. The antibiotic-resistant gene-expressing construct was connected with 5' and 3' homology arms by fusion PCR mediated with PrimeSTAR GXL DNA Polymerase (Takara Bio Inc., Shiga, Japan). The knockout construct was introduced into *A. limacinum* by electroporation with a Gene Pulser Xcell (Bio-Rad, Inc., CA, USA) (750 V, 25 μ F, 200 Ω). After being pulsed twice, 800 μ L of fresh GY medium was added. Cells were cultured at 25°C for 1 day and then transferred to a PDA plate containing 0.5 mg/mL of G418 or 1 mg/mL of hygromycin B (Wako Chemicals Inc., Osaka, Japan). The *dgat2* KO strains were selected and confirmed by PCR (Fig. S1D through F).

Lipid analysis

For TLC analysis, cells were cultured in GY medium at 25°C with shaking at 150 rpm for 3 or 8 days. Cells were collected by centrifugation (5,000 \times g, 3 min) then dried by lyophilization. Total lipid was extracted from 5 mg of the dried cell by adding 500 μ L of chloroform/methanol (2:1, vol/vol) with sonication. After incubation at 25°C for 10 min, samples were centrifuged at 17,500 \times g for 15 min, then 10 μ L of supernatant was loaded onto TLC, which was developed with hexane/diethyl ether/acetic acid (50/50/1 or 80/20/1, vol/vol/vol) for 10 min. Neutral lipids were visualized by spraying copper sulfate solution with heating at 120°C. For liquid chromatography-electrospray ionization-tandem mass spectrometry (LC-ESI MS/MS) analysis, cells were cultured in GY medium at 25°C with shaking at 150 rpm for an appropriate period, then 500 μ L of culture fluid was harvested. Cells were collected by centrifugation (5,000 \times g, 3 min), then the cell pellet was resuspended in 150- μ L distilled water, then crushed at 3,000 rpm for 60 s using a bead beater (μ T-12; TAITEC, Saitama, Japan) with glass beads (diameter: 0.6 mm, AS ONE Corp., Osaka, Japan) and kept on ice for 60 s. This procedure was repeated three times to prepare the cell lysate. Cellular lipids were extracted from 40 μ L of cell lysate by adding 160 μ L of chloroform/methanol (2:1, vol/vol) containing 10- μ M PC22:0 (C11:0/C11:0), 20- μ M DG24:0 (C12:0/C12:0), 10- μ M d7-C16:0-CE, and 20- μ M TG36:0 (C12:0/C12:0/C12:0).

as internal standards. After incubation at 37°C for 30 min, the mixture was centrifuged at $11,000 \times g$ for 3 min. Forty microliters of the organic phase was transferred to autoinjector vials containing 560 μL of 2-propanol, and then the cellular lipids were measured using LC-ESI MS/MS (3200 QTRAP; SCIEX, MA, USA). A binary solvent gradient with a 200- $\mu\text{L}/\text{min}$ flow rate was used to separate phospholipids and neutral lipids by reverse-phase chromatography using an InertSustain C18 column (2.1×150 mm, 5 μm ; GL Sciences, Japan) as described in references (19, 20). PC, DG, TG, and SE containing palmitic acid (C16:0) and DHA (C22:6) were detected using multiple reaction monitoring (MRM) as described in Table S2. For the analysis of TG and ergosterol ester (EE) of *dgat2c*- and *dgat2d*-expressing yeasts, palmitoleic acid- (C16:1) and oleic acid (C18:1)-containing molecular species were added to the MRM (Table S2). The signal values of each lipid were normalized with their corresponding internal standards. To measure the total sterol in *A. limacinum*, methanolysis using an acid catalyst [methanol containing 8% (wt/vol) HCl] was performed to release the esterified fatty acid of SE to generate a free form of sterols, as described in reference (21). The amount of free-form sterols was measured using liquid chromatography-atmospheric pressure chemical ionization (LC-APCI) MS/MS (3200 QTRAP) after separating sterols by a binary solvent gradient with an 800- $\mu\text{L}/\text{min}$ flow rate using an InertSustain C18 column (2.1×150 mm) started with 0% solvent B (methanol with 0.1% acetic acid) in solvent A (methanol/water = 96:4 containing 0.1% acetic acid) (22). The gradient reached 90% B over 4 min, then 100% B over 8 min, and was maintained for 2 min. The gradient was returned to the starting conditions, and the column was equilibrated for 4 min before the next run.

Assay of the *in vitro* TG synthase activity

WT and *dgat2d* KO strain were cultured until the glucose concentration of the medium reached approximately 0.5%. Two milliliters of the culture was collected and resuspended in 300 μL of 90-mM HEPES, pH 7.4, containing 0.02% Tween 20, and protease inhibitor cocktail (cOmplete Mini, Merck Millipore) then crushed by a beads beater. The amount of protein in the lysate was determined using a bicinchoninic acid protein assay (Thermo Fisher Scientific, USA). The cell lysate equivalent to 30 μg of protein was incubated in 60 μL of 15-mM Tris-HCl buffer, pH 7.5, containing 15 μM of [^{14}C]palmitoyl-CoA (0.1 mCi/mL, American Radiolabeled Chemicals Inc., USA), 25 mM of sucrose, 15 mM of KCl, 15 mM of MgCl_2 , and 125 $\mu\text{g}/\text{mL}$ of fatty acid-free bovine serum albumin (BSA) at 30°C for 10 min. The reaction was stopped by adding 300 μL of chloroform/methanol (2/1, vol/vol). The organic phase was evaporated under nitrogen gas, then resuspended in 10 μL of chloroform/methanol (2/1, vol/vol), then loaded onto TLC that was developed with hexane/diethyl ether/acetic acid (50/50/1, vol/vol/vol). The radioactivity was measured using an FLA 5100 Bio-imaging analyzer (GE Healthcare).

Generation of *dgat2c*-overexpressing mutants

To prepare the construct expressing FLAG-tagged *dgat2c*, PCR was performed using genomic DNA derived from *A. limacinum* mh0186 as a template and the primer described in Table S1. Inverse PCR using pEF-Neor/Ubi-mCherry as template DNA was performed to eliminate mCherry, which was located between the ubiquitin promoter and ubiquitin terminator derived from *Thraustochytrium aureum* to express the gene of interest in thraustochytrids, using primer set A.L_vector_Rv and A.L_vector_Fw (23) (Table S1). C-terminal FLAG-tagged *dgat2c* was inserted between the ubiquitin promoter and ubiquitin terminator of pEF-Neor/Ubi-mCherry instead of mCherry using an In-Fusion HD cloning kit (Takara Bio Inc.). The plasmid was used as a template to generate *dgat2c* mutants with truncated N-terminal predicted transmembrane regions (see Fig. 5A) amplified by PCR using primers listed in Table S1. To prepare the construct expressing N- or C-terminal green fluorescent protein (GFP)-fused DGAT2C or DGAT2D, PCR was performed using the primer set described in Table S1. The expression vector of enhanced GFP (EGFP) for thraustochytrids, pEF-Neor/Ubi-EGFP (pENUG) (23), was linearized by PCR using primers described in Table S1. The open reading frames (ORFs)

of *dgat2c* or *dgat2d* were inserted between *egfp* and ubiquitin terminator of pENUG to make N-terminal GFP-fused protein and between ubiquitin promoter and *egfp* of pENUG to make C-terminal GFP-fused protein using an In-Fusion HD cloning kit, respectively. The linearized expression construct was prepared by PCR using plasmid as a template, then introduced into *A. limacinum* mh0186 by electroporation using Gene Pulser Xcell (750 V, 25 μ F, 200 Ω). The transformants that grew on the PDA plate containing 0.5-mg/mL G418 were subjected to PCR screening.

Expression of *dgat2c* and *dgat2d* in *Saccharomyces cerevisiae*

The ORFs of *dgat2c* and *dgat2d* were amplified by PCR using genomic DNA of *A. limacinum* mh0186 and inserted into the MCS of pYES2/CT (Invitrogen, MA, USA). FLAG-tag was preadded to pYES2/CT, and *dgat2c* and *dgat2d* were expressed as C-terminal FLAG-tagged proteins. The expression plasmid vector of *dgat2c* was used as a PCR template to generate H642A and H644A mutant amplified using mutant primers listed in Table S1. The expression vectors were introduced into *S. cerevisiae* INVSc1 (Invitrogen) using the previously described method (24). The transformants were selected by plating on synthetic agar plates lacking uracil (SC-ura). *S. cerevisiae* transformants harboring *dgat2c* and *dgat2d* were cultured in SC-ura medium containing 2% glucose at 30°C for 1 day and cultured for an additional day in SC-ura medium containing 2% galactose. Next, 500 μ L of culture fluid was centrifuged at $1,500 \times g$ for 5 min to collect the cells and was used for the lipid analysis.

Quantitative real-time PCR

Total RNA was extracted from *A. limacinum* mh0186 after 5 days of culture using Sepasol-RNA I Super G (Nacalai Tesque) and an SV Total RNA Isolation System (Promega). cDNA was synthesized using a PrimeScript RT Reagent Kit with a gDNA Eraser (Perfect Real Time) (Takara Bio Inc.). Real-time PCR was performed using an Mx3000P qPCR System (Agilent Technologies) with SYBR Premix Ex Taq II (Tli RNaseH Plus) (Takara Bio Inc.) by using cDNA as a template. The numbers of copies of *dgat2a*, *dgat2c*, and *dgat2d* were determined using a plasmid containing each gene as a standard. Oligonucleotide primer sets for real-time PCR are shown in Table S1.

Western blotting analysis

To detect FLAG-tagged proteins in yeast and *A. limacinum*, 1 mL and 200 μ L of culture fluid were used, respectively. Cell pellets were suspended in PBS containing protease inhibitor cocktail and crushed by a beads beater with glass beads as described above. The amount of protein in the lysate was determined using a bicinchoninic acid protein assay. Equal amounts of proteins were subjected to 12.5% SDS-PAGE, followed by blotting onto a PVDF membrane using a Trans-Blot SD semi-dry transfer cell (Bio-Rad, Inc.). The membrane was blocked in Tris-buffered saline-Tween 20 (TBS-T) containing 5% BSA, then incubated with antibodies against DYKDDDDK tag (1:5,000) for over 12 h at 4°C. The membrane was washed with TBS-T and then incubated with HRP-conjugated anti-rabbit IgG antibody (1:10,000) (Cell Signaling Technology). The membrane was washed with TBS-T, and the protein was detected by chemiluminescence using Luminata Forte Western HRP substrate (Merck Millipore) and visualized with the use of a Cooled CCD Camera System Ez-Capture II (ATTO).

Assay of the *in vitro* SE synthase activity of DGAT2C

S. cerevisiae transformants harboring *dgat2c* or mock vector were cultured in 20 mL of SC-ura medium containing 2% glucose in a 50-mL flask at 30°C with shaking at 150 rpm for 1 day, and then cultured for an additional day in 40-mL SC-ura medium containing 2% galactose in a 100-mL flask. Twenty milliliters of the culture was centrifuged at $1,500 \times g$ for 5 min; then, cell pellets were dissolved in 300 μ L of PBS containing protease inhibitor cocktail and then crushed by a beads beater. The cell lysate was transferred to

a 1.5-mL tube and centrifuged at $1,000 \times g$ for 3 min. The supernatant was transferred to an ultracentrifuge tube, then centrifuged at $100,000 \times g$ for 1 h at 4°C to obtain the microsomal fraction. After removing the supernatant, the pellet was resuspended with sterile distilled water, then the protein concentration of the microsome was measured with a bicinchoninic acid protein assay. One hundred pmol of ergosterol was mixed with 300 nmol of sodium cholate. The mixture was sonicated for 30 s, and then the solvent was evaporated by a speed vac concentrator. The dried substrate was dissolved in 40 μL of 15 mM Tris-HCl buffer, pH 7.5, containing 33.3 μM of C22:6-CoA, 25 μM of sucrose, 15 μM of KCl, 15 μM of MgCl_2 , and 125 $\mu\text{g/mL}$ of fatty acid-free BSA with sonication (30 s). Finally, a microsomal fraction equivalent to 40 μg of protein was added to the substrate mixture, then incubated at 37°C with shaking at 1,500 rpm for 8 h. To determine the acyl donor of DGAT2C, 2 nmol of 1,2-didocosaheptaenoyl-*sn*-glycero-3-phosphocholine (C22:6 PC, Avanti Polar Lipids) or docosaheptaenoic acid (C22:6 free, Avanti Polar Lipids) was added to the reaction mixture instead of C22:6-CoA. The reaction was stopped by adding 400 μL of chloroform/methanol (2/1, vol/vol), and the sample was centrifuged ($11,000 \times g$ for 3 min). One hundred microliters of the organic phase was transferred to autoinjector vials containing 500 μL of 2-propanol, and then the product, C22:6-ergosterol ester (C22:6-EE), was measured using LC-ESI MS/MS.

Fluorescence microscopy

The N- or C-terminal GFP-fused DGAT2C or DGAT2D was observed under a fluorescence microscope, DMI8 with Leica Application Suite X (LAS X), equipped with an objective lens of $\times 100$ (numerical aperture 1.40) and a DFC3000G camera (Leica Microsystems, Wetzlar, Germany). LDs were stained by high-content screening LipidTOX Red neutral lipid stain, and nuclei were stained by Hoechst 33342 (Thermo Fisher Scientific).

Statistical analysis

All statistical analyses were performed using unpaired two-tailed Student *t*-tests, one-way or two-way analysis of variance with Tukey, and all data are expressed as means and standard deviations from at least three separate experiments. Statistical significance is indicated as follows: $*P < 0.05$, $**P < 0.01$, and $***P < 0.001$.

RESULTS

Genetic analysis of *dgat2a*, *dgat2c*, and *dgat2d* in *A. limacinum* mh0186

To elucidate the function of DGAT2 homologs in more detail, *dgat2a*, *dgat2c*, and *dgat2d* were disrupted in *A. limacinum* mh0186 (designated *dgat2a* KO, *dgat2c* KO, and *dgat2d* KO, respectively) (Fig. S1). LC-ESI MS/MS analysis showed that amounts of all molecular species of TG were dramatically reduced in the *dgat2d* KO (Fig. 1A). PC of *dgat2a*, *dgat2c*, and *dgat2d* KO was similar to that in the WT strain (Fig. 1B). In agreement with the reduction of TG, DG, which is a precursor for the synthesis of TG, was increased in *dgat2d* KO (Fig. S2A and B). In contrast, all molecular species of TG were not decreased in the *dgat2a* KO and *dgat2c* KO strains in comparison to those in the WT (Fig. 1A). Although DGAT2A has been reported to have TG synthetic activity (16), it seems that DGAT2A contributes little to the endogenous TG synthesis in *A. limacinum*. Importantly, the *in vitro* TG synthetic activity of cell lysate was markedly decreased in *dgat2d* KO, despite the presence of other *dgat2* homologs in this strain (Fig. 1C). These results indicate that DGAT2D is a major TG synthase that mainly contributes to the TG synthesis in *A. limacinum*, and other DGAT2 homologs are unable to compensate for the loss of DGAT2D function. The quantitative PCR showed that the mRNA expression level of *dgat2d* is significantly higher than that of other *dgat2* homologs (Fig. 1D), which is consistent with the result described in reference (16). This suggests that *dgat2* homologs with low expression levels are unlikely to reach sufficient transcript levels to compensate for the loss of *dgat2d*. The *dgat2d* KO strain showed a marked decrease in turbidity measured at OD600 and a delay in the consumption of glucose, the main carbon source in the

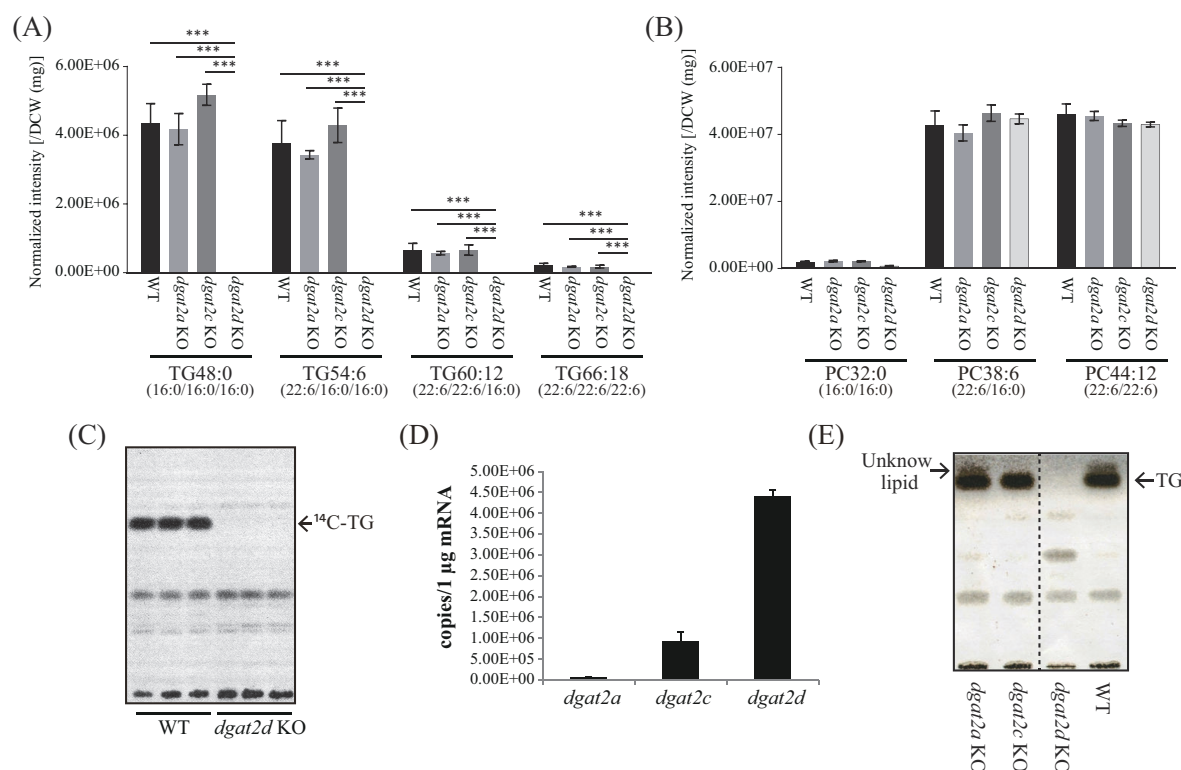


FIG 1 Lipid profile of *dgat2a*, *dgat2c*, and *dgat2d* KO strains. Quantification of each molecular species of TG (A) and PC (B) of WT, *dgat2a*, *dgat2c*, and *dgat2d* KO strains harvested from 3-day cultures. The results of panels A and B were obtained by LC-ESI MS/MS analysis (MRM mode). The peak intensity of each lipid was normalized with dry cell weight (DCW). Data represent means \pm SDs of three separate experiments. Statistical significance is indicated as follows: *** $P < 0.001$. (C) *In vitro* TG synthase activity of WT and *dgat2d* KO strain. TG synthase activity was measured using ^{14}C -labeled palmitoyl-CoA as a donor substrate, and cell lysate as an enzyme and acceptor substrate (DG) source, as described in Materials and Methods. (D) mRNA expression levels of *dgat2a*, *dgat2c*, and *dgat2d*. A standard curve to determine the copy numbers of each gene was generated from various concentrations of plasmid containing the DNA sequence of *dgat2a*, *dgat2c*, and *dgat2d*, respectively. (E) TLC analysis showing the neutral lipid profiles of *dgat2a*, *dgat2c*, *dgat2d* KO strains and WT. Total lipids were extracted from cells cultured for 8 days. Lipid extracts were applied to a TLC plate that was developed with hexane/diethyl ether/acetic acid = 50/50/1 (vol/vol/vol). Neutral lipids were visualized by spraying copper sulfate solution. Noncontiguous portions of the same TLC are indicated by dashed lines.

culture medium, indicating that disruption of *dgat2d* causes the severe growth defect in *A. limacinum* (Fig. S3A and B). On the other hand, the growth of *dgat2a* KO and *dgat2c* KO strains was almost identical to that of the WT (Fig. S3C and D), suggesting that TG synthesis could be important for *A. limacinum* for normal growth. Since TG synthetic activity was almost completely abolished by *dgat2d* KO (Fig. 1C), we consider that the reduction of TG was due to the loss of TG synthesis mediated by DGAT2D, rather than the growth defect in the *dgat2d* KO strain.

In agreement with LC-ESI MS/MS result, TLC analysis revealed that the band corresponding to TG disappeared in *dgat2d* KO, while the band remained unchanged in the WT, *dgat2a* KO, and *dgat2c* KO (Fig. 1E). We found that an unknown lipid whose R_f is faster than TG on the TLC detected in the WT disappeared in the *dgat2c* KO (Fig. 1E). To identify this unknown lipid, MS analysis of lipids from the WT, *dgat2c* KO, and *dgat2c* KO/*dgat2c* OE, which is the strain that *dgat2c* was reintroduced in the *dgat2c* KO, were performed. Consequently, the intensity of the spectra corresponding to $m/z = 714.6$ was significantly reduced, and that corresponding to $m/z = 738.6$ and 740.6 lost in the *dgat2c* KO compared to the WT and *dgat2c* KO/*dgat2c* OE (Fig. 2A). Tandem mass spectrometry (MS/MS) analysis revealed that the $m/z = 740.6$ and 738.6 spectra were derived from $\Delta 7$ -stigmasterol-ester ($\Delta 7$ -SE) containing docosapentaenoic acid (C22:5- $\Delta 7$ -SE) and DHA (C22:6- $\Delta 7$ -SE), respectively, and that of $m/z = 714.6$ was from cholesterol ester (CE) containing DHA (C22:6-CE), because fragment ion $m/z = 393.4$ derived from

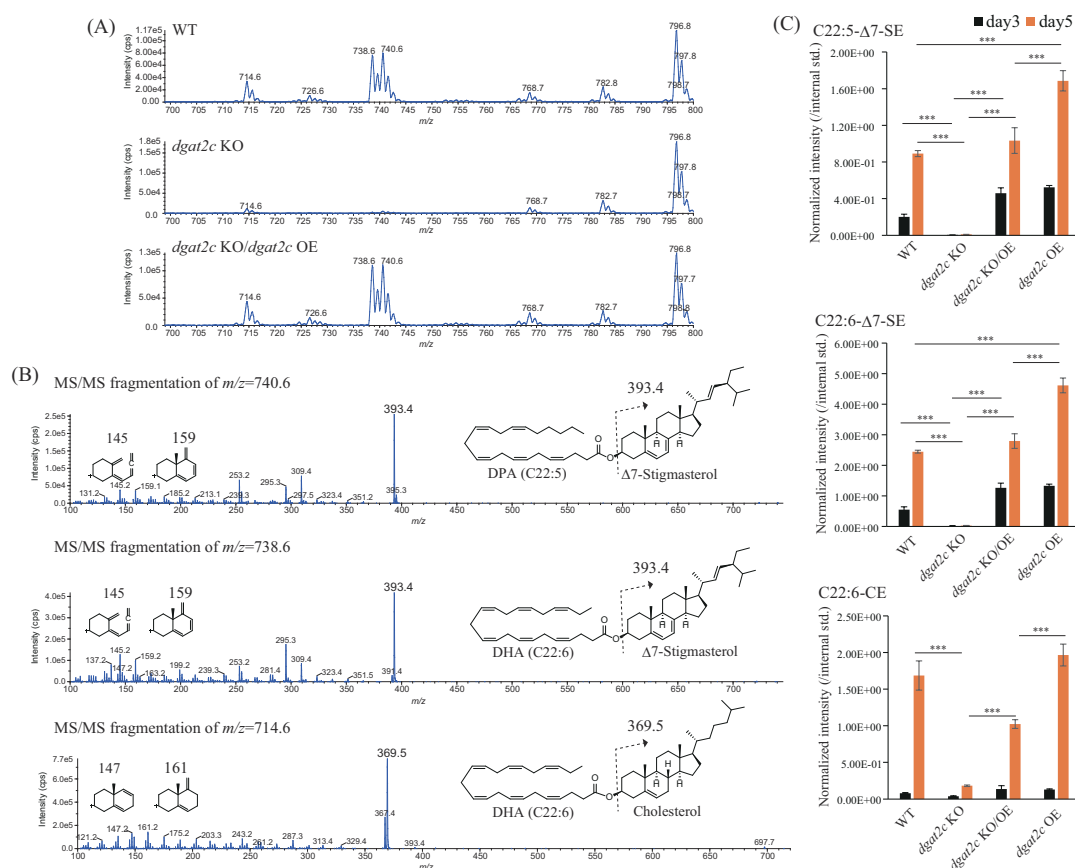


FIG 2 Structural analysis of lipids lost in the *dgat2c* KO strain of *A. limacinum* mh0186. (A) Positive ion MS spectra of SE that were lost in the *dgat2c* KO strain. The spectrum shows that $m/z = 740.6$ and 738.6 were ablated in the *dgat2c* KO strain. In comparison with that of the WT, the intensity of $m/z = 714.6$ decreased in the *dgat2c* KO strain. The intensities of these spectra were recovered by the reintroduction of *dgat2c* into the *dgat2c* KO strain. (B) MS/MS fragmentation spectra of $m/z = 740.6$, 738.6 , and 714.6 . Structure-specific fragment ions are generated in MS/MS, depending on the number of the double bond in ring B of sterol moieties of SE. According to their MS/MS fragmentation pattern, $m/z = 740.6$, 738.6 , and 714.6 were identified as docosapentaenoic acid (DPA, C22:5)- Δ^7 -stigmasterol ester (C22:5- Δ^7 -SE), C22:6- Δ^7 -stigmasterol ester (C22:6- Δ^7 -SE), and C22:6-cholesterol ester (C22:6-CE), respectively. (C) Quantification of SE of the WT, *dgat2c* KO, *dgat2c* KO/*dgat2c* OE, and *dgat2c* OE strains. The cellular C22:5- Δ^7 -SE, C22:6- Δ^7 -SE, and C22:6-CE levels of each strain were measured using LC-ESI MS/MS (MRM mode) at the indicated time points. Data represent means \pm SDs of three separate experiments. The peak intensity of each lipid was normalized with that of the internal standard. Statistical significance is indicated as follows: *** $P < 0.001$.

precursor ions $m/z = 740.6$ and 738.6 was assigned to Δ^7 -stigmasterol (25), and $m/z = 369.5$ derived from precursor ion $m/z = 714.6$ was assigned to cholesterol in the MS/MS analysis (Fig. 2B). These results were supported by detecting the fragment ions $m/z = 145$ and $m/z = 159$ that were derived from double bonds at Δ^5 and Δ^7 of the B-ring in Δ^7 -stigmasterol (Fig. 2B), and the fragment ions $m/z = 147$ and $m/z = 161$ that were derived from a single double bond at Δ^5 of the B-ring in cholesterol (Fig. 2B) (26). The amounts of polyunsaturated fatty acid (PUFA)-containing SE drastically decreased in the *dgat2c* KO in comparison to the WT and *dgat2c* KO/OE (Fig. 2C). In contrast to DHA, palmitic acid (C16:0) is rarely incorporated into SE in *A. limacinum* mh0186 (Fig. S4). These results indicate that DGAT2C is involved in PUFA-containing SE synthesis in *A. limacinum* mh0186. Subsequently, the *dgat2c* was overexpressed in the WT (*dgat2c* OE strain) to further understand the function of DGAT2C. The amounts of SE, particularly C22:5- Δ^7 -SE and C22:6- Δ^7 -SE, increased in the *dgat2c* OE cultured for 5 days (Fig. 2C).

***In vivo* and *in vitro* assays of DGAT2C after heterologous expression in budding yeast**

Rau et al. reported that dysfunction of ALASATb, which was found as a DGAT2 homolog, significantly reduced the intracellular SE level in *A. limacinum* SR21 and suggested that ALASATb was an acyl-CoA:sterol-O-acyltransferase (ASAT) (27). To further understand the functions of DGAT2 homologs, the C-terminal FLAG-tagged *dgat2c* and *dgat2d* were expressed in *S. cerevisiae*, and their expressions were examined by Western blotting using an anti-FLAG-tag antibody. DGAT2D (60.7 kDa) and DGAT2C (99.9 kDa) were detected with the expected molecular weight, indicating that these genes are properly expressed in *S. cerevisiae* (Fig. 3A). The amount of TG increased in the *dgat2d*-expressing strain (pYES-*dgat2d*), while that of the *dgat2c*-expressing strain (pYES-*dgat2c*) was almost the same as that of the empty vector expressing strain of *S. cerevisiae* (mock) (Fig. S5). In the mock strain, C16:1-EE and C18:1-EE, but not C16:0-EE and C18:0-EE, were detected (Fig. 3B) due to the specificity of yeast SE synthase (Are1/2) and endogenous sterol pool in *S. cerevisiae*; i.e., Are1/2 prefers monounsaturated fatty acids such as palmitoleic acid (C16:1) and oleic acid (C18:1), and the major sterol pool in *S. cerevisiae* is ergosterol (28). In contrast to the mock, C16:0-EE and C18:0-EE significantly increased in pYES-*dgat2c*, but not pYES-*dgat2d* (Fig. 3B), indicating that DGAT2C has an SE synthase activity with different specificity from Are1/2 of *S. cerevisiae*. Next, the SE synthase activity was examined *in vitro* using the microsomal fraction of pYES-*dgat2c* as an enzyme source. C22:6-EE was detected when the microsomal fraction of pYES-*dgat2c*, but not the mock, was incubated with C22:6-CoA (Fig. 3C and D). However, a free form of DHA [C22:6 (free)] or DHA-containing PC (C22:6-PC) was not a donor substrate for DGAT2C (Fig. 3D). Taken together, *in vivo* and *in vitro* experiments using *S. cerevisiae* clarified that DGAT2C is an SE synthase that uses acyl-CoA as a donor substrate, and, thus, the systematic name of DGAT2C should be ASAT, although the primary structure is more homologous to DGAT2 than to known ASATs.

Identification of catalytic residue of DGAT2C

The HPHG motif conserved in all DGAT2 family members is required for the enzymatic activity of DGAT2; thus, this motif is considered a part of the active site (29). This motif is conserved in DGAT2D and DGAT2C (Fig. 3E). Because DGAT2C is the first DGAT2 that uses sterols as acceptor substrates, whether this motif is essential for enzyme activity, such as conventional DGAT2, is unclear. Since histidine residue is known to be involved in catalysis in DGAT1 (29), the first and third residues in the HPHG motif of DGAT2C were replaced with alanine (H642A and H644A), respectively, and the activity of each mutant was compared with the WT enzyme. Although the protein expression level of the H644A mutant enzyme (H644A) was almost the same as that of DGAT2C (WT) in *S. cerevisiae* (Fig. 3F), C16:0-EE and C18:0-EE, which were synthesized by DGAT2C (WT), were not detected in the H644A-expressing strain, similarly to the mock transfectant (Fig. 3G). On the other hand, C16:0-EE and C18:0-EE were synthesized in an H642A-expressing strain despite lower protein expression level compared to WT and H644A (Fig. 3F and G), suggesting that the first residue (histidine) of the HPHG is not involved in the catalyst of DGAT2C but might contribute to the protein stability of DGAT2C. Taken together, our results indicate that the third residue (histidine) of the HPHG motif is essential for the ASAT activity of DGAT2C similar to the conventional DGAT2.

Different intracellular localization of DGAT2C and DGAT2D

As described above, two DGAT2 homologs, DGAT2C and DGAT2D, possess completely different substrate specificities; i.e., the former is an SE synthase, and the latter is a TG synthase. To clarify the intracellular localization of these two enzymes, each EGFP-fused protein was expressed in *A. limacinum* mh0186. First, EGFP fused to the N-terminal of DGAT2C (GFP-DGAT2C) and that to the C-terminal of DGAT2C (DGAT2C-GFP) were expressed in *dgat2c* KO (*dgat2c* KO/*gfp-dgat2c* OE and *dgat2c* KO/*dgat2c-gfp* OE), and

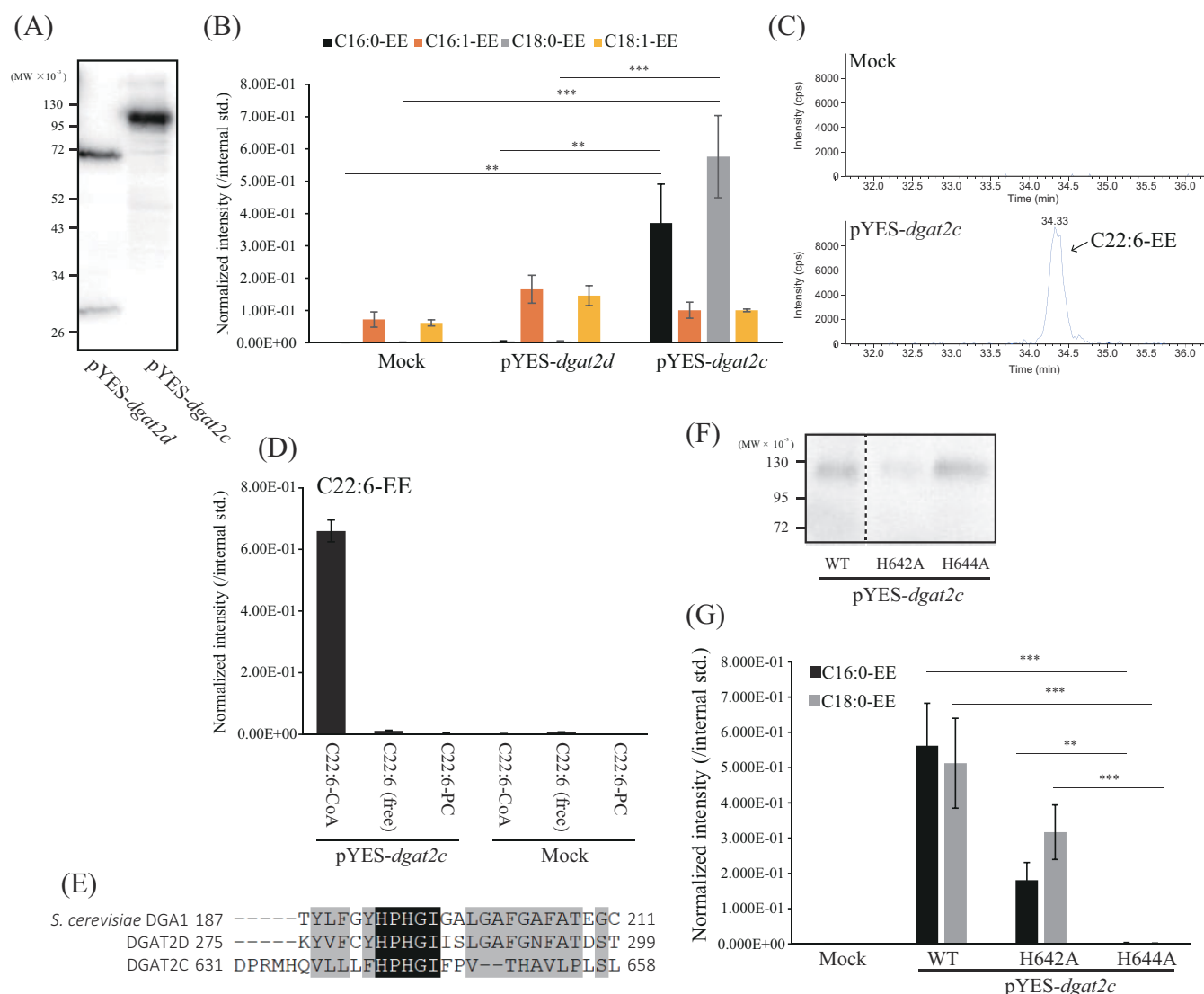


FIG 3 *In vivo* and *in vitro* assays of DGAT2C after heterologous expression in budding yeast. (A) Western blotting showing the expression of DGAT2D and DGAT2C in *S. cerevisiae*. The C-terminal FLAG-tagged DGAT2D and DGAT2C were expressed in *S. cerevisiae* using the pYES vector. After induction of protein expression by galactose, cells were collected and crushed by a bead beater. Cell lysates were subjected to Western blotting using an antibody against FLAG-tag. (B) Quantification of cellular ergosterol-ester (EE) levels of mock, *dgat2d*, and *dgat2c*-expressing *S. cerevisiae*. EE containing C16:0, C16:1, C18:0, and C18:1 of each strain was measured by LC-ESI MS/MS (MRM mode). (C) *In vitro* SE synthetic activity of DGAT2C expressed in *S. cerevisiae*. The microsomal fractions equivalent to 40 μ g of protein derived from the mock and *dgat2c*-expressing strains were mixed with ergosterol and C22:6-CoA, as described in the Materials and Methods. After incubation at 37°C for 8 h, an appropriate amount of chloroform/methanol = 2/1 (vol/vol) was added to the reaction solutions. The organic phase containing SE was applied to LC-ESI MS/MS (MRM mode) analysis to detect C22:6-EE. (D) Identification of the acyl donor substrate for the esterified fatty acid of SE synthesis by DGAT2C. The same amount of C22:6-CoA, free form of C22:6 [C22:6 (free)], or PC comprising C22:6 (C22:6-PC) was incubated with microsomal fractions of the mock and *dgat2c*-expressing yeast to reveal the acyl donor of DGAT2C. (E) Multiple alignments of amino acid sequences around the HPHG motif, which is conserved in the DGAT2 family enzyme, of DGA1 (TG synthase of *S. cerevisiae*), DGAT2D, and DGAT2C. (F) Western blot showing the expression levels of the WT, H642A, and H644A mutants of DGAT2C in *S. cerevisiae*. Noncontiguous portions of the same membrane are indicated by dashed lines. (G) Quantification of EE levels of the mock, *dgat2c* (WT)-, *dgat2c* (H642A)-, and *dgat2c* (H644A)-expressing *S. cerevisiae*. Data represent means \pm SDs of three separate experiments. The peak intensity of each lipid was normalized with that of the internal standard. Statistical significance is indicated as follows: ** $P < 0.01$, and *** $P < 0.001$.

each SE productivity was examined to verify the effect of EGFP fusion on enzyme activity. GFP-DGAT2C showed a similar SE productivity to the intact DGAT2C; however, DGAT2C-GFP decreased the SE productivity, indicating that the fusion of EGFP to the C-terminal

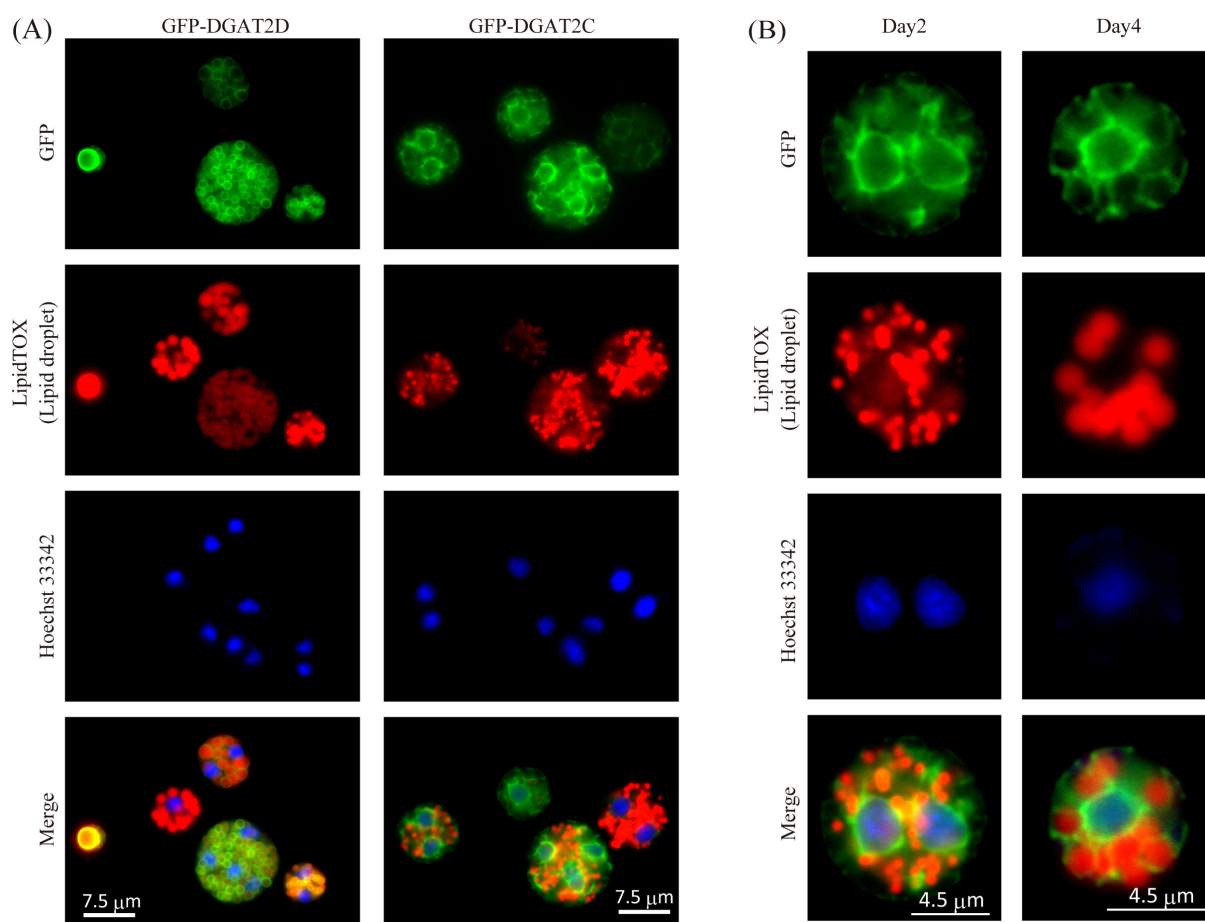


FIG 4 Intracellular localization of GFP-DGAT2D and GFP-DGAT2C in *A. limacinum* mh0186. (A) Localization of GFP-DGAT2D and GFP-DGAT2C. EGFP was fused with the N-terminal of DGAT2D or DGAT2C, respectively. GFP-DGAT2D- and GFP-DGAT2C-expressing constructs were integrated into the genomic DNA of *A. limacinum* mh0186 and stably expressed by the ubiquitin promoter. (B) Localization of DGAT2C in different culture periods. LDs were stained with high-content screening LipidTOX Red neutral lipid stain, and Hoechst 33342 was used for staining nuclei.

end may affect the function and stability of DGAT2C (Fig. S6). Therefore, the localization of DGAT2 was examined using N-terminal EGFP-fusion proteins in this study.

It was found that N-terminal EGFP-DGAT2D localized to the LD, while N-terminal EGFP-DGAT2C localized to the ER, which is the organelle encircling the nuclei (Fig. 4A). Although LDs grew and became larger on day 4, localization of N-terminal EGFP-DGAT2C on the ER was unchanged on days 2 and 4 of culture (Fig. 4B). The localization of N-terminal EGFP-DGAT2C is very similar to that of EGFP with ER retention signal (23), and DGAT2C was estimated to localize to the ER by MulocDEEP localization prediction based on its primary structure (30). These results indicate that TG and SE are synthesized at different organelles by DGAT2D and DGAT2C, respectively, in *A. limacinum* mh0186.

Analysis of N-terminal deletion mutants of DGAT2C

To disclose the molecular mechanism which makes the difference in substrate specificity and localization of DGAT2C and DGAT2D, we generated five N-terminal deletion mutants in which two putative transmembrane regions were deleted from the N-terminal of DGAT2C (Fig. 5) because DGAT2C possesses 10 more putative transmembrane regions on the N-terminal side than DGAT2D (Fig. 5A; Fig. S7A and B). We expressed these deletion mutants of DGAT2C in *dgat2c* KO of *A. limacinum* mh0186 (Δ TM1-2, Δ TM1-4, Δ TM1-6, Δ TM1-8, and Δ TM1-10 *dgat2c* strains). LC-ESI MS/MS analysis revealed that production of C22:6-CE (Fig. 5B) and C22:6- Δ 7-SE (Fig. S8) was maintained in deletion mutant strains

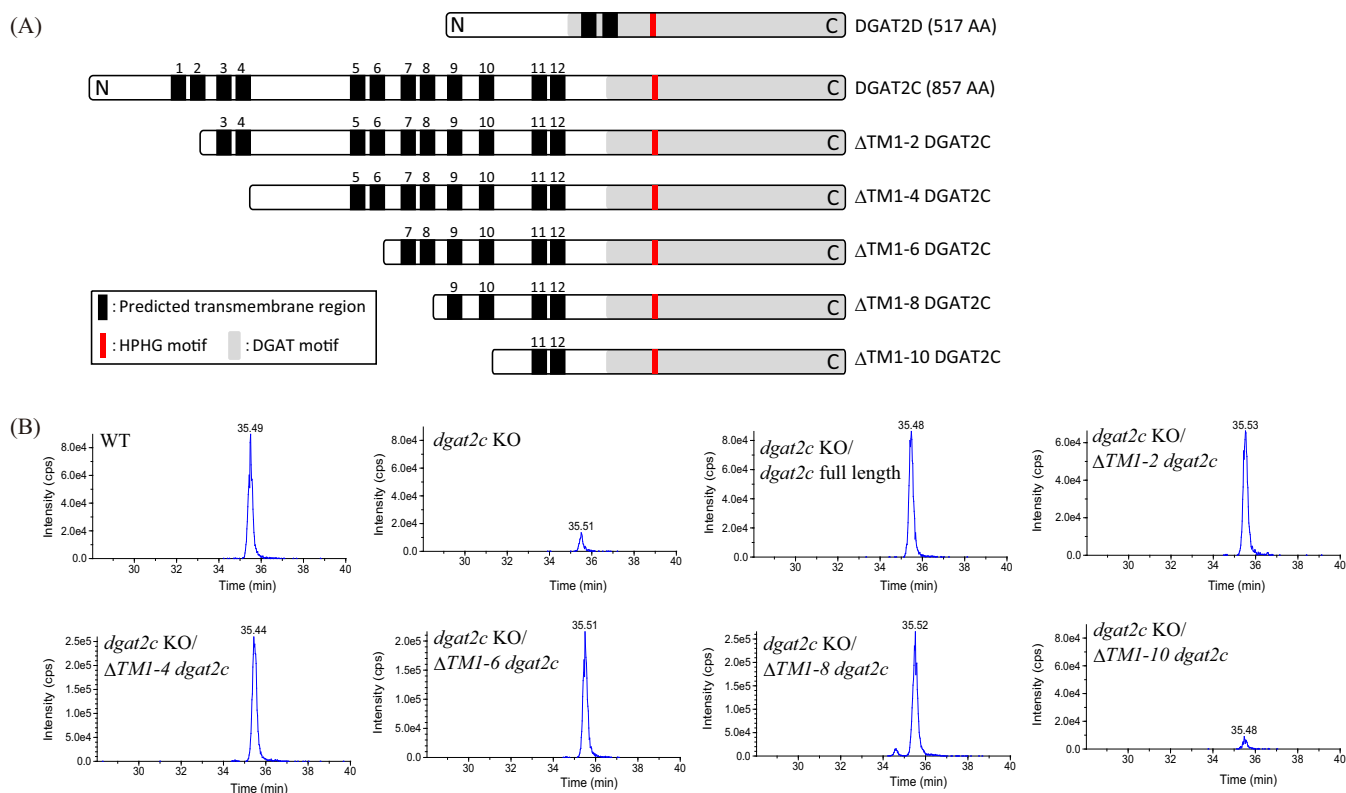


FIG 5 SE synthase activity in N-terminal deletion mutants of DGAT2C. (A) Structural schematics of DGAT2D and DGAT2C showing the putative transmembrane regions, catalytic HPHG motif, and DGAT motif. In comparison with DGAT2D, DGAT2C has unique 12 putative transmembrane regions. To evaluate the function of the N-terminal of DGAT2C, each of the two putative transmembrane regions was deleted from the N-terminal in a graded manner to make a series of deletion mutants, Δ TM1-2, Δ TM1-4, Δ TM1-6, Δ TM1-8, and Δ TM1-10 DGAT2C. (B) Chromatogram of C22:6-CE of each strain detected by LC-ESI MS/MS analysis. A series of N-terminal-truncated mutants of *dgat2c* were reintroduced into the *dgat2c* KO strain, and their SE synthetic abilities were verified using LC-ESI MS/MS (MRM mode).

except for the Δ TM1-10 *dgat2c* strain, indicating that the sequence containing the 9th and 10th putative transmembrane regions is indispensable for the SE synthase activity of DGAT2C. Δ TM1-2, Δ TM1-4, Δ TM1-6, and Δ TM1-8 DGAT2C localized to the ER, such as full-length DGAT2C (Fig. 6). Alternatively, Δ TM1-10 DGAT2C did not localize to the ER (Fig. 6) and showed similar localization of EGFP alone, which localizes at cytosol (23). The sequence containing the 9th and 10th putative transmembrane regions is essential for SE production and ER localization of DGAT2C in *A. limacinum* mh0186.

The function of the N-terminal region of DGAT2C

This study indicates that the N-terminal region containing the first to the eighth putative transmembrane regions was not required for SE production and ER localization of DGAT2C in *A. limacinum* mh0186. To elucidate the function of the N-terminal region, C-terminal flag-tagged, full-length Δ TM1-8 and Δ TM1-10 *dgat2c* were expressed in the *dgat2c* KO of *A. limacinum* mh0186 (full-length *dgat2c*, Δ TM1-8 *dgat2c*, and Δ TM1-10 *dgat2c* strains, respectively), and their SE production and protein expression levels were examined. Interestingly, the amounts of SE markedly increased in the Δ TM1-8 *dgat2c* strain compared to those in the WT and full-length *dgat2c* strain during the culture period (Fig. 7A). However, the Δ TM1-10 *dgat2c* strain showed no production of C22:6-CE and C22:6-ΔSE (Fig. 7A). Conversely, the amount of TG comprising three DHA (TG66:18) decreased significantly in the Δ TM1-8 *dgat2c* strain (Fig. 7B), suggesting that DHA is used for SE synthesis instead of TG because of high SE synthase activity in the Δ TM1-8 *dgat2c* strain. The increase in SE and the decrease in TG in the Δ TM1-8 *dgat2c* strain

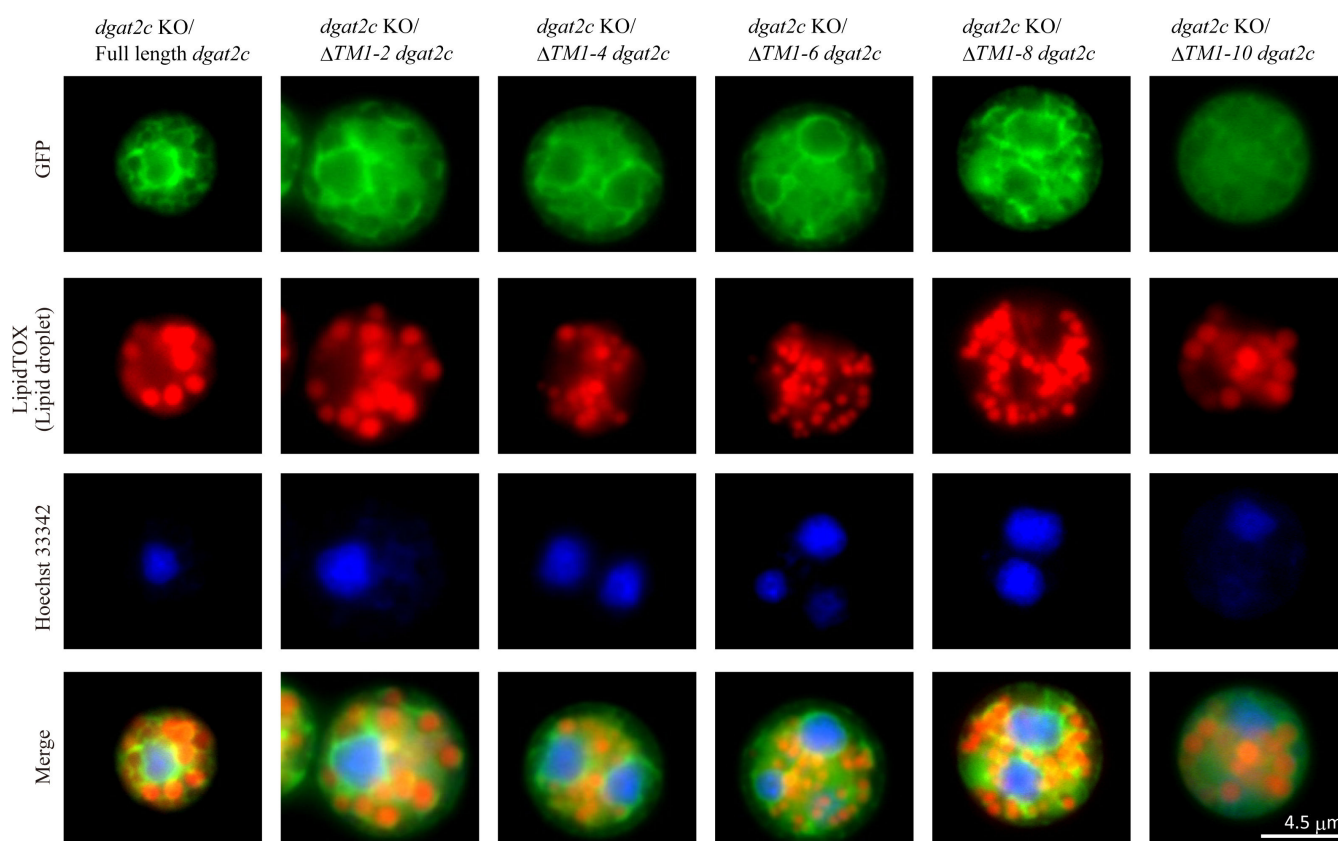


FIG 6 Localization of N-terminal deletion mutants of DGAT2C in *A. limacinum* mh0186. N-terminal EGFP-fused, full-length Δ TM1-2, Δ TM1-4, Δ TM1-6, Δ TM1-8, and Δ TM1-10 *dgat2c* were expressed in the *dgat2c* KO strain of *A. limacinum* mh0186. LDs were stained with high-content screening LipidTOX red neutral lipid stain, and Hoechst 33342 was used for staining nuclei.

were also confirmed using TLC analysis (Fig. 7C). No significant difference was observed in the EE level when the Δ TM1-8, full-length, or Δ TM1-6 *dgat2c* was expressed in *S. cerevisiae* (Fig. S9A). Western blot analysis revealed that the Δ TM1-8 DGAT2C expression was significantly higher than that of full-length or Δ TM1-10 DGAT2C when expressed in the *dgat2c* KO strain of *A. limacinum* (Fig. 7D). These results suggested that the increase in SE production in the Δ TM1-8 *dgat2c* strain is at least in part due to high DGAT2C expression in *A. limacinum*. An increase in DGAT2C expression and SE production was not observed in the Δ TM1-6 DGAT2C strain, and thus, the amino acid sequence containing the seventh and eighth transmembrane regions may be important for controlling the expression of DGAT2C in *A. limacinum* (Fig. S9B and C).

Next, the amount of free sterol level in the Δ TM1-8 *dgat2c* strain was measured by LC-APCI MS/MS analysis before and after methanolysis with hydrochloric acid (Fig. S10A). In contrast to SE, the amount of free sterol without methanolysis decreased in the Δ TM1-8 *dgat2c* strain compared to that in the WT or other mutant strains (Fig. S10B), suggesting that free sterol pools were used more for SE synthesis in the Δ TM1-8 *dgat2c* strain. Alternatively, the cholesterol and Δ 7-stigmasterol amounts in this mutant strain drastically increased after methanolysis, reaching three times higher levels than those of the WT strain (Fig. 7E). This result indicates that the total sterol amount drastically increased in the Δ TM1-8 *dgat2c* strain compared to that in the WT strain.

In the cholesterol synthesis pathway, Δ 7-cholesterol (7-dehydrocholesterol) is a precursor of cholesterol (Fig. 8A). The C7-C8 double bond in the B ring of Δ 7-cholesterol is reduced by 7-dehydrocholesterol reductase (DHCR7) to generate cholesterol. Because Δ 7-cholesterol is converted to vitamin D3 by ultraviolet B, Δ 7-cholesterol is called provitamin D3. Δ 7-Cholesterol and Δ 7-cholesterol-ester were rarely detected in

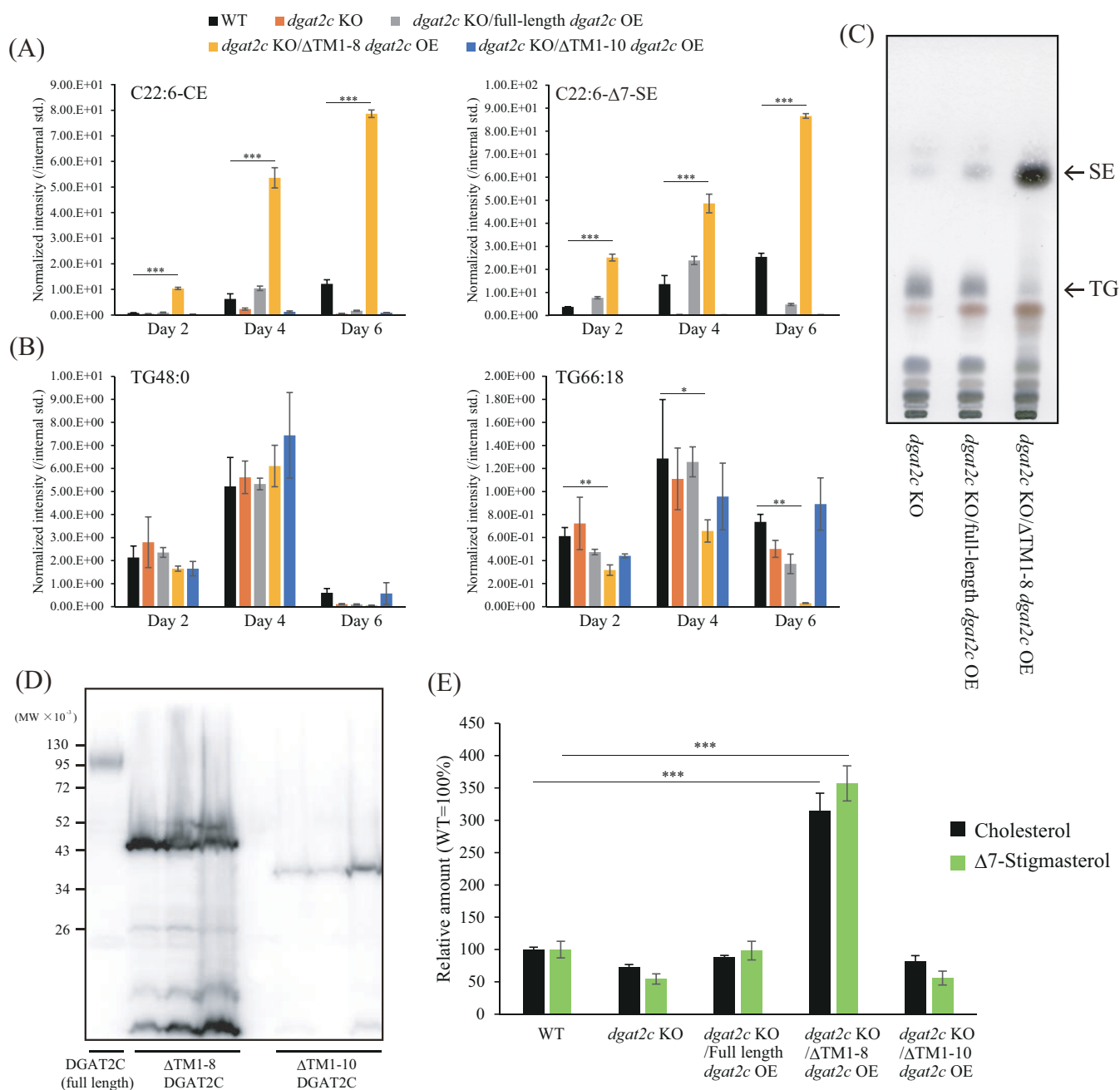


FIG 7 Increase in SE and total sterol amounts in *A. limacinum* mh0186 by ΔTM1-8 DGAT2C expression. (A) Quantification of C22:6-CE (left panel) and C22:6-Δ7-SE (right panel) of WT, *dgat2c* KO, *dgat2c* KO/full-length *dgat2c* OE, *dgat2c* KO/ΔTM1-8 *dgat2c* OE, and *dgat2c* KO/ΔTM1-10 *dgat2c* OE strains. (B) Quantification of TG48:0 (C16:0/C16:0/C16:0, left panel) and TG66:18 (C22:6/C22:6/C22:6, right panel) of the same strains described in panel A. The cellular C22:6-CE, C22:6-Δ7-SE, TG48:0, and TG66:18 levels of each strain were measured using LC-ESI MS/MS (MRM mode) at the indicated time points. The full-length, ΔTM1-8, and ΔTM1-10 *dgat2c* were reintroduced into the *dgat2c* KO strain. The peak intensity of each lipid was normalized with that of the internal standard. (C) TLC analysis showing the neutral lipid profiles of *dgat2c* KO, *dgat2c* KO/full-length *dgat2c* OE, and *dgat2c* KO/ΔTM1-8 *dgat2c* OE strains. Lipid extracts were applied to a TLC plate that was developed with hexane/diethyl ether/acetic acid = 80/20/1 (vol/vol/vol). Neutral lipids were visualized by spraying copper sulfate solution. (D) Western blotting showing the protein expression levels of full-length DGAT2C, ΔTM1-8 DGAT2C and ΔTM1-10 DGAT2C. The molecular mass of full-length, ΔTM1-8 and ΔTM1-10 DGAT2C is estimated to be 98.8, 53.1, and 39.1 kDa, respectively. Three independent ΔTM1-8- and ΔTM1-10 *dgat2c*-expressing strains were obtained and applied to Western blotting analysis. (E) Quantification of total sterol of the WT, *dgat2c* KO, *dgat2c* KO/full-length *dgat2c* OE, *dgat2c* KO/ΔTM1-8 *dgat2c* OE, and *dgat2c* KO/ΔTM1-10 *dgat2c* OE strains. The total of the free form of sterols was measured using LC-APCI MS/MS (MRM mode) after releasing sterols from SE by methanolysis. The relative amount with the WT as 100% of cholesterol and Δ7-stigmasterol is calculated. Data represent means ± SDs of three separate experiments. Statistical significance is indicated as follows: * $P < 0.05$, ** $P < 0.01$, and *** $P < 0.001$.

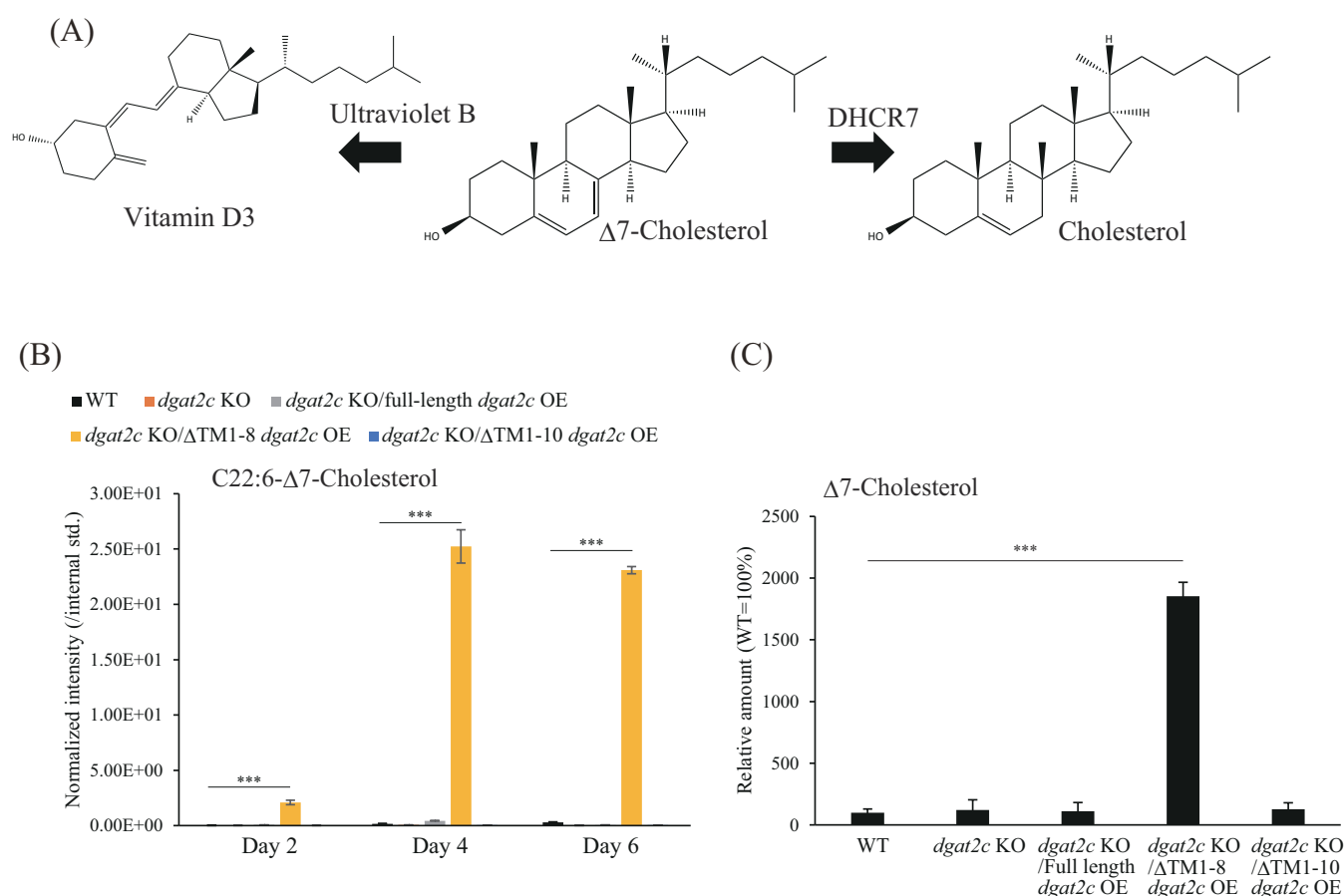


FIG 8 Production of provitamin D3 ester (Δ^7 -cholesterol ester) in *A. limacinum* mh0186 by Δ TM1-8 DGAT2C expression. (A) Correlation between cholesterol, Δ^7 -cholesterol, and vitamin D3 in the synthetic pathway of cholesterol. The double bond at the Δ^7 position in ring B of Δ^7 -cholesterol is reduced by DHCR7 to generate cholesterol. Vitamin D3 is generated from Δ^7 -cholesterol by irradiation of ultraviolet B. (B) Quantification of Δ^7 -cholesterol ester composed of C22:6 (C22:6- Δ^7 -cholesterol) of the WT, *dgat2c* KO, *dgat2c* KO/full-length *dgat2c* OE, *dgat2c* KO/ Δ TM1-8 *dgat2c* OE, and *dgat2c* KO/ Δ TM1-10 *dgat2c* OE strains. The cellular C22:6- Δ^7 -cholesterol level of each strain was measured using LC-ESI MS/MS (MRM mode) at the indicated time points. The peak intensity of each lipid was normalized with that of the internal standard. (C) Quantification of total Δ^7 -cholesterol. The total amount of Δ^7 -cholesterol was measured using LC-APCI MS/MS (MRM mode) after releasing sterol from SE by methanolysis. The relative amount with the WT as 100% is calculated. Data represent means \pm SDs of three separate experiments. Statistical significance is indicated as follows: *** $P < 0.001$.

the WT of *A. limacinum* during the course of the culture period (Fig. 8B and C; Fig. S11A). We found that a substantial amount of Δ^7 -cholesterol-ester containing C22:6 (C22:6- Δ^7 -cholesterol) was produced in the Δ TM1-8 *dgat2c* strain cultured for 4 and 7 days (Fig. 8B). The m/z 712.5, which is derived from C22:6- Δ^7 -cholesterol, was detected only in the Δ TM1-8 *dgat2c* strain (Fig. S11A), and the structure of C22:6- Δ^7 -cholesterol was confirmed by the MS/MS analysis, in which fragment ions 145 and 159 derived from double bonds at Δ^5 and Δ^7 of the B-ring in Δ^7 -cholesterol were detected (26) (Fig. S11B), respectively. Consistent with the accumulation of C22:6- Δ^7 -cholesterol, the total amount of Δ^7 -cholesterol drastically increased in the Δ TM1-8 *dgat2c* strain (Fig. 8C). These results indicated that Δ TM1-8 DGAT2C expression is useful for high production of Δ^7 -stigmasterol, cholesterol and Δ^7 -cholesterol that are rarely synthesized in *A. limacinum*.

DISCUSSION

This study indicated that two DGAT2 homologs in *A. limacinum* mh0186 use different acceptor substrates; i.e., DGAT2C and DGAT2D use sterols and DG as acceptor substrates to generate SE and TG, respectively. Rau et al. reported that AlASATb of *A. limacinum* SR21, whose sequence is very close to that of DGAT2C of *A. limacinum* mh0186, could

be an SE synthase by knockout and overexpression of *alasatb* in *A. limacinum* SR21 (27). In addition to the genetic approach in *A. limacinum*, we showed that DGAT2C synthesizes SE from acyl-CoA and sterols by heterologous expression of *dgat2c* in budding yeast using an *in vitro* enzyme assay. Furthermore, we successfully developed a method to increase sterol production in the thraustochytrid by elucidating the function of the DGAT2C-specific N-terminal region. The mutant strain expressing Δ TM1-8 DGAT2C enabled the production of cholesterol and Δ 7-stigmasterol more than three times that of WT *A. limacinum* (Fig. 7E). These results are expected to be a clue of the practical application of sterol production using thraustochytrids in the future.

The growth characteristic of the *dgat2d* KO was different from that of the *dgat2a* and *dgat2c* KO mutant strains (Fig. S3). WT cells showed a maximum TG level when they reached the stationary phase (day 4), followed by a decrease in the decline phase (day 6) (Fig. 7B; Fig. S3A and B), suggesting that TG is stored in LD as an alternative energy resource to survive after external carbon sources such as glucose are exhausted in the medium (Fig. S3C and D). Thus, we expected that the loss of TG in *dgat2d* KO may cause a difference in OD600 after the stationary phase. However, the OD600 values of *dgat2d* KO had already decreased in the early stages of the culture, despite the presence of sufficient glucose in the medium (Fig. 2A and B). Our result suggests that TG may have other important biological functions besides simply being a nutrient storage for *A. limacinum*, but the details are unknown.

Fluorescent microscopy analysis using EGFP-fused DGAT2 homologs revealed that DGAT2C is entirely different in localization from DGAT2D, i.e., the former localizes to the ER and the latter to the LDs in *A. limacinum* mh0186 (Fig. 4). LD proteins are divided into Classes I and II (31, 32). Class I proteins originally localize to the ER and then move to the LDs during the formation and maturation of LDs. Alternatively, Class II proteins directly localize to the LDs from the cytoplasm. DGAT2D is likely a Class I protein because it is predicted to localize to the ER from its primary structure. Although DGAT2D is speculated to have two transmembrane regions, as shown in Fig. 5A, DGAT2D appears to be a monotopic protein that enters the membrane region but does not penetrate to the opposite side (Fig. S12A). Monotopic proteins are stably incorporated into the membrane via hydrophobic hairpin domain, forming a topology in which the soluble domain is exposed toward one side of the membrane. In many cases, proline residues at the midpoint of the hydrophobic regions break the helix structure to form a hairpin domain. The presence of proline at the center of the helical domain of DGAT2D supports that DGAT2D has a hydrophobic hairpin domain (Fig. S12A) and localizes to the LDs as a monotopic protein. In contrast to DGAT2D, DGAT2C localized to the ER but not to the LDs during the culture period (Fig. 4A and B). Although Δ TM1-8 DGAT2C localized to the ER, Δ TM1-10 DGAT2C did not (Fig. 6), suggesting that the 9th and 10th putative transmembrane regions are real transmembrane regions, which enter the ER membrane (Fig. S12B).

In agreement with the study by Rau et al. (27), DHA is the main fatty acid linked to sterols in *A. limacinum* (Fig. S4), suggesting that DGAT2C may prefer DHA-CoA over saturated fatty acyl-CoA. However, the experiment of heterologous expression in yeast revealed that 16:0-EE and 18:0-EE were synthesized by DGAT2C, indicating that DGAT2C has a broad substrate specificity and can utilize not only DHA-CoA but also saturated fatty acyl-CoA. Thus, we wonder why DHA-containing SE was selectively synthesized in *A. limacinum*. Similar to DGAT2C, PC synthase, PLAT1, which is estimated to localize at ER, synthesizes significantly more DHA-containing PCs (PC38:6 and PC44:12) than PCs containing only saturated fatty acids (PC32:0) in *A. limacinum*. However, it has no specificity for fatty acyl-CoA species (33). These results indicate that DHA-CoA is more accessible than palmitoyl-CoA for ER-localized enzymes, leading to preferentially synthesized DHA-containing SE or PC.

The C-terminal region of DGAT2C has a DGAT motif that shows high similarities with DGAT2D (Fig. 5; Fig. S12). The HPHG sequence, which is essential for the activity of DGAT2-like enzymes, is also conserved in the C-terminal DGAT motif in DGAT2C.

The third residue (histidine) in the HPGH motif is demonstrated to be integral to the SE synthase activity of DGAT2C (Fig. 3G). This result suggests that the mechanism for synthesizing SE by DGAT2C is partly similar to that of TG by conventional DGAT2, although DGAT2C utilizes sterol instead of DG as an acceptor substrate. As shown in the three-dimensional structure of mammalian ACAT1 that transfers fatty acid from acyl-CoA to cholesterol, transmembrane regions are involved in sterol recognition (34). Thus, we hypothesized that the unique substrate specificity of DGAT2C could be dependent on 12 putative transmembrane regions in the N-terminal region that are not present in DGAT2D (Fig. 5A). In this study, we showed that the 1st to 8th transmembrane regions of DGAT2C are not essential for SE production in *A. limacinum*, suggesting that the 9th to 12th transmembrane regions would be involved in recognizing sterol (Fig. S12B). Importantly, these transmembrane regions are also conserved in DGAT2C of thraustochytrids other than *A. limacinum* (Fig. S13) but not in DGAT2 homologs of other eukaryotes. Thus, DGAT2C is considered a unique SE synthase specifically acquired in thraustochytrids during their evolution.

Surprisingly, the Δ TM1-8 *dgat2c* strain showed a significant increase in SE, leading to a threefold increase in total cholesterol and Δ 7-stigmasterol compared to the WT strain of *A. limacinum* mh0186 (Fig. 7E). Furthermore, Δ 7-cholesterol and Δ 7-cholesterol-SE, which are rarely detected in the WT, were generated in the Δ TM1-8 *dgat2c* strain (Fig. 8B and C). The demand for sterols and SE has been increasing because of their usefulness; thus, a sustainable source for sterol production is required. As described in the Introduction, phytosterols have biological benefits such as anti-inflammatory, anti-oxidant, and anti-cancer activities. Cholesterol and Δ 7-cholesterol are a precursor for the steroid hormone ecdysterone, which regulates molting, growth, and immune response in crustaceans (35). In addition, cholesterol can stimulate the synthesis of sex hormones, promote gonadal development, and facilitate crustacean reproduction and fecundity (36). Since the *de novo* synthetic pathway of cholesterol is lost in crustaceans, cholesterol in feed is necessary for shrimp aquaculture (37). Thraustochytrids are evaluated as a sustainable aquaculture feed alternative to fishmeal and fish oil because they can synthesize n-3PUFA, which is indispensable for the growth of marine fish (38). In addition to fish aquaculture, cholesterol and Δ 7-cholesterol production-potentiated thraustochytrid are expected to be used for shrimp aquaculture.

The major reason for the increase in SE content when Δ TM1-8 DGAT2C was expressed in *dgat2c*-deficient *A. limacinum* was likely due to the increase in Δ TM1-8 DGAT2C expression at the protein level (Fig. 7D). This could be due to the presence of the region that negatively regulates the expression or promotes the degradation of DGAT2C in the first to the eighth putative transmembrane regions. We might be able to rule out the possibility that the enzymatic activity of DGAT2C *per se* was increased by deleting the putative transmembrane region since no significant increase in SE synthesis was observed in Δ TM1-8 *dgat2c* expression in budding yeast (Fig. S9A).

Δ 7-Cholesterol, provitamin D3, is converted to vitamin D3 by ultraviolet B in sunlight (39). Fractures and bone loss have been linked to vitamin D deficiency. Severe vitamin D deficiency significantly increases the risk of infection and many other diseases (40). Approximately 40% of Europeans are suggested to have a vitamin D deficiency, and 13% have a severe deficiency (41). Vitamin D has rare side effects, a wide safety margin, and pathophysiological links with energy homeostasis, immune system function, and endocrine regulation (40). The individual patient data meta-analysis of randomized placebo-controlled trials to evaluate vitamin D's effect on cancer mortality indicated that daily vitamin D supplementation could reduce cancer mortality by 12% (42). Thus, vitamin D is an important, safe, and inexpensive adjunctive therapy for multiple diseases, particularly cancer. Supplementation with vitamin D is recommended because sunlight exposure and dietary intake are often insufficient to maintain optimal vitamin D status (40). The growing awareness of vitamin D has led to an increase in the use of vitamin D supplements and the expansion of its market (43). Recent attempts have been made to produce vitamin D3 using thraustochytrid because of its high sterol productivity. For the

production of $\Delta 7$ -cholesterol, DHCR7, which converts $\Delta 7$ -cholesterol to cholesterol (Fig. 8A), is deleted in *Aurantiochytrium* sp (44). In this study, we successfully developed a new method that significantly increases the production of $\Delta 7$ -cholesterol. It is expected to lead to a higher production of vitamin D3 in *A. limacinum* by combining these different strategies synergistically.

Prediction of localization of DHCR7 based on its sequence in *A. limacinum* indicates that it is likely to localize to the ER similarly with DGAT2C. $\Delta 7$ -Cholesterol would be converted to $\Delta 7$ -cholesterol ester by Δ TM1-8 DGAT2C before being converted to cholesterol by DHCR7 because of the high expression of Δ TM1-8 DGAT2C, then $\Delta 7$ -cholesterol ester finally accumulates in LDs where no reduction in $\Delta 7$ -cholesterol occurs. Δ TM1-8 DGAT2C expression in *A. limacinum* produced $\Delta 7$ -cholesterol ester and unknown SE that was eluted before C22:6- $\Delta 7$ -SE on LC (Fig. S8), indicating that Δ TM1-8 DGAT2C could utilize intermediate(s) other than $\Delta 7$ -cholesterol to generate their SE.

This study disclosed more detailed properties and the localization of DGAT2C, a unique SE synthase in thraustochytrids. We found that the expression of a mutant enzyme that appropriately truncated the N-terminal region of DGAT2C could increase the SE content and, thus, the total sterol content in *A. limacinum* mh0186. This finding is expected to be one of the cornerstones for future industrial production of sterols using thraustochytrids.

ACKNOWLEDGMENTS

This study was supported in part by a Grant-in-Aid for Young Scientists (B) (JP15K18740) and Grant-in-Aid for Scientific Research (C) (21K06034) from the Japanese Ministry of Education, Culture, Sports, Science, and Technology. R.T. was supported by JST Global Science Campus from the Japan Science and Technology Agency.

Conceptualization: Y.I.; conducting the experiments: Y.I., S.S., Y.F., Y.Y., and R.T.; data analysis: Y.I., S.S., and Y.F.; supervision: N.O. and T. W.; resources: M.H.; writing: Y. I. and M.I. All authors reviewed the results and approved the final version of the manuscript.

AUTHOR AFFILIATIONS

¹Department of Bioscience and Biotechnology, Graduate School of Bioresource and Bioenvironmental Sciences, Kyushu University, Fukuoka, Japan

²Kyushu University Future Creators in Science Project (QFC-SP), Fukuoka, Japan

³Department of Marine Biology and Environmental Sciences, Faculty of Agriculture, University of Miyazaki, Miyazaki, Japan

AUTHOR ORCIDS

Yohei Ishibashi  <http://orcid.org/0000-0002-9657-8207>

FUNDING

Funder	Grant(s)	Author(s)
MEXT Japan Society for the Promotion of Science (JSPS)	JP15K18740, 21K06034	Yohei Ishibashi
MEXT Japan Science and Technology Agency (JST)	JST Global Science Campus	Rin Tanogashira

AUTHOR CONTRIBUTIONS

Yohei Ishibashi, Conceptualization, Data curation, Formal analysis, Funding acquisition, Investigation, Methodology, Project administration, Supervision, Visualization, Writing – original draft | Shohei Sadamitsu, Data curation, Investigation | Yoshitomo Fukahori, Investigation, Resources | Yuki Yamamoto, Investigation, Resources | Rin Tanogashira, Investigation | Takashi Watanabe, Methodology | Masahiro Hayashi, Resources | Makoto

Ito, Supervision, Writing – review and editing | Nozomu Okino, Supervision, Writing – review and editing

ADDITIONAL FILES

The following material is available [online](#).

Supplemental Material

Supplemental tables and figures (AEM01001-23-S0001.pdf). This file includes supplemental tables (S1 and S2) and supplemental figures (S1 - S13).

REFERENCES

- Barenholz Y. 2002. Cholesterol and other membrane active sterols: from membrane evolution to "rafts" *Prog Lipid Res* 41:1–5. [https://doi.org/10.1016/S0163-7827\(01\)00016-9](https://doi.org/10.1016/S0163-7827(01)00016-9)
- Hannan MA, Sohag AAM, Dash R, Haque MN, Mohibullah M, Oktaviani DF, Hossain MT, Choi HJ, Moon IS. 2020. Phytosterols of marine algae: insights into the potential health benefits and molecular pharmacology. *Phytomedicine* 69:153201. <https://doi.org/10.1016/j.phymed.2020.153201>
- Stamler J, Daviglus ML, Garside DB, Dyer AR, Greenland P, Neaton JD. 2000. Relationship of baseline serum cholesterol levels in 3 large cohorts of younger men to long-term coronary, cardiovascular, and all-cause mortality and to longevity. *JAMA* 284:311–318. <https://doi.org/10.1001/jama.284.3.311>
- Moreau RA, Nyström L, Whitaker BD, Winkler-Moser JK, Baer DJ, Gebauer SK, Hicks KB. 2018. Phytosterols and their derivatives: structural diversity, distribution, metabolism, analysis, and health-promoting uses. *Prog Lipid Res* 70:35–61. <https://doi.org/10.1016/j.plipres.2018.04.001>
- Randhir A, Laird DW, Maker G, Trengove R, Moheimani NR. 2020. Microalgae: a potential sustainable commercial source of sterols. *Algal Research* 46:101772. <https://doi.org/10.1016/j.algal.2019.101772>
- Hou X, Zaks T, Langer R, Dong Y. 2021. Lipid nanoparticles for mRNA delivery. *Nat Rev Mater* 6:1078–1094. <https://doi.org/10.1038/s41578-021-00358-0>
- Yokoyama R, Honda D. 2007. Taxonomic rearrangement of the genus *Schizochytrium* sensu lato based on morphology, chemotaxonomic characteristics, and 18S rRNA gene phylogeny (Thraustochytriaceae, Labyrinthulomycetes): emendation for *Schizochytrium* and erection of *Aurantiochytrium* and *Oblongichytrium* gen. nov. *Mycoscience* 48:199–211.
- Yokoyama R, Salleh B, Honda D. 2007. Taxonomic rearrangement of the genus *Ulkenia* sensu lato based on morphology, chemotaxonomical characteristics, and 18S rRNA gene phylogeny (Thraustochytriaceae, Labyrinthulomycetes): emendation for *Ulkenia* and erection of *Botryochytrium*, *Parietichytrium*, and *Sicyoidochytrium* gen. nov. *Mycoscience* 48:329–341. <https://doi.org/10.1007/S10267-007-0377-1>
- Morabito C, Bournaud C, Maës C, Schuler M, Aiese Cigliano R, Dellerio Y, Maréchal E, Amato A, Rébeillé F. 2019. The lipid metabolism in thraustochytrids. *Prog Lipid Res* 76:101007. <https://doi.org/10.1016/j.plipres.2019.101007>
- Orozco Colonia BS, Vinícius de Melo Pereira G, Soccol CR. 2020. Omega-3 microbial oils from marine thraustochytrids as a sustainable and technological solution: a review and patent landscape. *Trends Food Sci* 99:244–256. <https://doi.org/10.1016/j.tifs.2020.03.007>
- Dellerio Y, Cagnac O, Rose S, Seddiki K, Cussac M, Morabito C, Lupette J, Aiese Cigliano R, Sanseverino W, Kuntz M, Jouhet J, Maréchal E, Rébeillé F, Amato A. 2018. Proposal of a new thraustochytrid genus *Hondaia* gen. nov. and comparison of its lipid dynamics with the closely related pseudo-cryptic genus *Aurantiochytrium*. *Algal Research* 35:125–141. <https://doi.org/10.1016/j.algal.2018.08.018>
- Yoneda K, Ishibashi Y, Yoshida M, Watanabe MM, Ito M, Suzuki I. 2022. Proteomic and lipidomic analyses of lipid droplets in *Aurantiochytrium limacinum* ATCC MYA-1381. *Algal Research* 67:102844. <https://doi.org/10.1016/j.algal.2022.102844>
- Gupta A, Barrow CJ, Puri M. 2022. Multiproduct biorefinery from marine thraustochytrids towards a circular bioeconomy. *Trends Biotechnol* 40:448–462. <https://doi.org/10.1016/j.tibtech.2021.09.003>
- Shokravi H, Shokravi Z, Heidarrezaei M, Ong HC, Rahimian Koor SS, Petrú M, Lau WJ, Ismail AF. 2021. Fourth generation biofuel from genetically modified algal biomass: challenges and future directions. *Chemosphere* 285:131535. <https://doi.org/10.1016/j.chemosphere.2021.131535>
- Chen G, Harwood JL, Lemieux MJ, Stone SJ, Weselake RJ. 2022. Acyl-CoA:diacylglycerol acyltransferase: properties, physiological roles, metabolic engineering and intentional control. *Prog Lipid Res* 88:101181. <https://doi.org/10.1016/j.plipres.2022.101181>
- Lan C, Wang S, Zhang H, Wang Z, Wan W, Liu H, Hu Y, Cui Q, Song X. 2021. Cocktail biosynthesis of triacylglycerol by rational modulation of diacylglycerol acyltransferases in industrial oleaginous *Aurantiochytrium*. *Biotechnol Biofuels* 14:246. <https://doi.org/10.1186/s13068-021-02096-5>
- Nagano N, Taoka Y, Honda D, Hayashi M. 2009. Optimization of culture conditions for growth and docosahexaenoic acid production by a marine thraustochytrid, *Aurantiochytrium limacinum* mh0186. *J Oleo Sci* 58:623–628. <https://doi.org/10.5650/jos.58.623>
- Sakaguchi K, Matsuda T, Kobayashi T, Ohara JI, Hamaguchi R, Abe E, Nagano N, Hayashi M, Ueda M, Honda D, Okita Y, Taoka Y, Sugimoto S, Okino N, Ito M. 2012. Versatile transformation system that is applicable to both multiple transgene expression and gene targeting for thraustochytrids. *Appl Environ Microbiol* 78:3193–3202. <https://doi.org/10.1128/AEM.07129-11>
- Watanabe T, Sakiyama R, Iimi Y, Sekine S, Abe E, Nomura KH, Nomura K, Ishibashi Y, Okino N, Hayashi M, Ito M. 2017. Regulation of TG accumulation and lipid droplet morphology by the novel TLDPI in *Aurantiochytrium limacinum* F26-B. *J Lipid Res* 58:2334–2347. <https://doi.org/10.1194/jlr.M079897>
- Ikeda K, Oike Y, Shimizu T, Taguchi R. 2009. Global analysis of triacylglycerols including oxidized molecular species by reverse-phase high resolution LC/ESI-QTOF MS/MS. *J Chromatogr B Analyt Technol Biomed Life Sci* 877:2639–2647. <https://doi.org/10.1016/j.jchromb.2009.03.047>
- Ichihara K, Fukubayashi Y. 2010. Preparation of fatty acid methyl esters for gas-liquid chromatography. *J Lipid Res* 51:635–640. <https://doi.org/10.1194/jlr.D001065>
- McDonald JG, Smith DD, Stiles AR, Russell DW. 2012. A comprehensive method for extraction and quantitative analysis of sterols and secosteroids from human plasma. *J Lipid Res* 53:1399–1409. <https://doi.org/10.1194/jlr.D022285>
- Okino N, Wakisaka H, Ishibashi Y, Ito M. 2018. Visualization of Endoplasmic Reticulum and mitochondria in *Aurantiochytrium limacinum* by the expression of EGFP with cell organelle-specific targeting/retaining signals. *Mar Biotechnol* 20:182–192. <https://doi.org/10.1007/s10126-018-9795-7>
- Ito H, Fukuda Y, Murata K, Kimura A. 1983. Transformation of intact yeast cells treated with alkali cations. *J Bacteriol* 153:163–168. <https://doi.org/10.1128/jb.153.1.163-168.1983>
- Endo I, Watanabe T, Miyamoto T, Monjusho-Goda H, Ohara J, Hayashi M, Hama Y, Ishibashi Y, Okino N, Ito M. 2021. C4-monomethylsterol β -glucoside and its synthase in *Aurantiochytrium limacinum* Mh0186. *Glycobiology* 31:1350–1363. <https://doi.org/10.1093/glycob/cwab070>
- Münger LH, Boulos S, Nyström L. 2018. UPLC-MS/MS based identification of dietary sterol glucosides by investigation of corresponding free sterols. *Front Chem* 6:342. <https://doi.org/10.3389/fchem.2018.00342>

27. Rau EM, Bartosova Z, Kristiansen KA, Aasen IM, Bruheim P, Ertesvåg H. 2022. Overexpression of two new Acyl-CoA:Diacylglycerol Acyltransferase 2-like Acyl-CoA:Sterol Acyltransferases enhanced squalene accumulation in *Aurantiochytrium limacinum* Front Microbiol 13:822254. <https://doi.org/10.3389/fmicb.2022.822254>
28. Zweytick D, Leitner E, Kohlwein SD, Yu C, Rothblatt J, Daum G. 2000. Contribution of Are1p and Are2p to sterol ester synthesis in the yeast *Saccharomyces cerevisiae*. Eur J Biochem 267:1075–1082. <https://doi.org/10.1046/j.1432-1327.2000.01103.x>
29. Stone SJ, Levin MC, Farese RV Jr. 2006. Membrane topology and identification of key functional amino acid residues of murine Acyl-CoA:Diacylglycerol Acyltransferase-2. J Biol Chem 281:40273–40282. <https://doi.org/10.1074/jbc.M607986200>
30. Jiang Y, Wang D, Yao Y, Eubel H, Künzler P, Möller IM, Xu D. 2021. Mulocdeep: a deep-learning framework for protein subcellular and suborganellar localization prediction with residue-level interpretation. Comput Struct Biotechnol J 19:4825–4839. <https://doi.org/10.1016/j.csbj.2021.08.027>
31. Kory N, Farese RV, Walther TC. 2016. Targeting fat: mechanisms of protein localization to lipid droplets. Trends Cell Biol 26:535–546. <https://doi.org/10.1016/j.tcb.2016.02.007>
32. Dhiman R, Caesar S, Thiam AR, Schrüf B. 2020. Mechanisms of protein targeting to lipid droplets: a unified cell biological and biophysical perspective. Semin Cell Dev Biol 108:4–13. <https://doi.org/10.1016/j.semcdb.2020.03.004>
33. Abe E, Ikeda K, Nutahara E, Hayashi M, Yamashita A, Taguchi R, Doi K, Honda D, Okino N, Ito M. 2014. Novel lysophospholipid acyltransferase PLAT1 of *Aurantiochytrium limacinum* F26-b responsible for generation of Palmitate-Docosahexaenoate-Phosphatidylcholine and Phosphatidylethanolamine. PLoS One 9:e102377. <https://doi.org/10.1371/journal.pone.0102377>
34. Qian H, Zhao X, Yan R, Yao X, Gao S, Sun X, Du X, Yang H, Wong CCL, Yan N. 2020. Structural basis for catalysis and substrate specificity of human ACAT1 structural determination of ACAT1. Nature 581:333–338. <https://doi.org/10.1038/s41586-020-2290-0>
35. Mykles DL. 2011. Ecdysteroid metabolism in crustaceans. J Steroid Biochem Mol Biol 127:196–203. <https://doi.org/10.1016/j.jsbmb.2010.09.001>
36. Kumar V, Sinha AK, Romano N, Allen KM, Bowman BA, Thompson KR, Tidwell JH. 2018. Metabolism and nutritive role of cholesterol in the growth, gonadal development, and reproduction of crustaceans. Rev Fish Sci Aquac 26:254–273. <https://doi.org/10.1080/23308249.2018.1429384>
37. Kanazawa A. 2001. Sterols in marine invertebrates. Fisheries Sci 67:997–1007. <https://doi.org/10.1046/j.1444-2906.2001.00354.x>
38. Chi G, Xu Y, Cao X, Li Z, Cao M, Chisti Y, He N. 2022. Production of polyunsaturated fatty acids by *Schizochytrium (Aurantiochytrium)* spp. Biotechnol Adv 55:107897. <https://doi.org/10.1016/j.biotechadv.2021.107897>
39. Deluca HF. 2014. History of the discovery of vitamin D and its active metabolites. Bonekey Rep 3:479. <https://doi.org/10.1038/bonekey.2013.213>
40. Amrein K, Scherkl M, Hoffmann M, Neuwersch-Sommeregger S, Köstenberger M, Tmava Berisha A, Martucci G, Pilz S, Malle O. 2020. Vitamin D deficiency 2.0: an update on the current status worldwide. Eur J Clin Nutr 74:1498–1513. <https://doi.org/10.1038/s41430-020-0558-y>
41. Cashman KD, Dowling KG, Škrabáková Z, Gonzalez-Gross M, Valtuena J, De Henauw S, Moreno L, Damsgaard CT, Michaelsen KF, Mølgaard C, Jorde R, Grimnes G, Moschonis G, Mavrogianni C, Manios Y, Thamm M, Mensink GB, Rabenberg M, Busch MA, Cox L, Meadows S, Goldberg G, Prentice A, Dekker JM, Nijpels G, Pilz S, Swart KM, van Schoor NM, Lips P, Eiriksdottir G, Gudnason V, Cotch MF, Koskinen S, Lamberg-Allardt C, Durazo-Arvizu RA, Sempos CT, Kiely M. 2016. Vitamin D deficiency in Europe: pandemic? Am J Clin Nutr 103:1033–1044. <https://doi.org/10.3945/ajcn.115.120873>
42. Kuznia S, Zhu A, Akutsu T, Buring JE, Camargo CA, Cook NR, Chen L-J, Cheng T-Y, Hantunen S, Lee I-M, Manson JE, Neale RE, Scragg R, Shadyab AH, Sha S, Sluyter J, Tuomainen T-P, Urashima M, Virtanen JK, Voutilainen A, Wactawski-Wende J, Waterhouse M, Brenner H, Schöttker B. 2023. Efficacy of vitamin D3 supplementation on cancer mortality: systematic review and individual patient data meta-analysis of randomised controlled trials. Ageing Res Rev 87:101923. <https://doi.org/10.1016/j.arr.2023.101923>
43. Arora N, Philippidis GP. 2023. The prospects of algae-derived vitamins and their precursors for sustainable cosmeceuticals. Processes 11:587. <https://doi.org/10.3390/pr11020587>
44. Ujihara T, Mitsuhashi S. 2015. Manufacturing method for 7-dehydrocholesterol and vitamin D3. WO/2015/108058